MONITORING OF GLASS TRANSITION AT A POLYMER SURFACE BY LOCALIZED SURFACE PLASMON RESONANCE

By

RATAN KISHORE PUTLA

Bachelor of Technology in Mechanical Engineering

Jawaharlal Nehru Technological University

Hyderabad, India

2006

Submitted to the Faculty of the
Graduate College of the
Oklahoma State University
in partial fulfillment of
the requirements for
the Degree of
MASTER OF SCIENCE
December, 2010

MONITORING OF GLASS TRANSITION AT A POLYMER

SURFACE BY LOCALIZED SURFACE

PLASMON RESONANCE

Thesis Approved:

Dr. A. Kaan Kalkan

Assistant Professor of Mechanical and Aerospace Engineering
Thesis Adviser

Dr. Sandip P. Harimkar

Assistant Professor of Mechanical and Aerospace Engineering
Committee Member

Dr. Ranji Vaidyanathan

Herrington Professor of Advanced Materials
Committee Member

Dr. Mark E. Payton

Dean of the Graduate College

ACKNOWLEDGMENTS

I am very thankful to my adviser Dr. A. Kaan Kalkan for offering me a very exciting project and guiding me through it with valuable inputs in the form of teaching, explaining and directing in the concepts that form the backbone for my research. I am also thankful to Dr. Hongbing Lu, Dr. Sandip P. Harimkar and Dr. Ranji Vaidyanathan for their valuable time spent in giving me their invaluable suggestions and feedback.

I also thank Dr. A. Lloyd Bumm of Physics and Astronomy Department, University of Oklahoma for helping me with valuable inputs in advanced spectroscopy. I am also pleased to acknowledge all my colleagues of the Functional Nanomaterials Laboratory for their support and encouragement. I would also like to acknowledge NASA, NSF, TBag and Ocast for supporting my research work.

I take this opportunity to thank my beloved dad & mom, uncle & aunt, sisters and brother-in-law for their prayers, moral support and great encouragement.

Above all, I sincerely thank, owe and dedicate this research work to my beloved **FATHER JESUS** without **WHOSE** help I would never been able to reach this level in my life. I thank **HIM** for **HIS** constant encouragement, moral support and being my driving force throughout this research work.

TABLE OF CONTENTS

LIST OF TABLES

Table **Page**

LIST OF FIGURES

Figure **Page**

CHAPTER 1

INTRODUCTION

A surface can be defined as a transition region between one medium and another and is different from region 1 and region 2. The properties at the surface deviate from those in the bulk due to broken and strained bonds as well as reduced density of atoms/molecules. Particularly in polymers, these deviations at the surface substantially impact the mechanical properties [1 - 4]. One such mechanical property is the glass transition temperature (T_g) [5, 6]. Investigations on polymer surfaces by various groups revealed that the surface T_g (T_{gs}) is not equal to the bulk T_g (T_{gb}) [7, 8]. While some groups claim that T_{gs} of a polymer is lower than T_{gb} [9 - 11], others claim that T_{gs} is higher than T_{gb} [12]. Yet, some other groups claim that there is no difference between T_{gs} and T_{gb} [13, 14].

In 2001, Zaporojtchenko , Strunskus, Erichsen and Faupel introduced a new technique for probing the T_{gs} of a polymer by the embedding of noble metal nanoparticles [23]. Later in 2003, Teichroeb and Forrest imaged

embedding of gold nanoparticles into polystyrene surface by atomic force microscopy. They suggested that there is a more mobile surface region of about 3-4 nm thick, indicative of a lower T_g at the surface compared to the bulk [15]. However, in 2005 Hutcheson and McKenna presented an interpretation contrary to the results of Teichroeb and Forrest using a visco-elastic contact mechanics model [16, 17]. According to Hutcheson and McKenna, the embedding of gold nanoparticles was due to the indentation created by the large surface interaction between polystyrene and gold. Hence, they concluded that there is no possible existence of a so called "liquid layer" as proposed by Teichroeb and Forrest [16, 17]. After the controversy raised by these studies, it is understood that a better understanding of T_g of a polymer at its surface has yet to be attained.

In the present work however, instead of atomic force microscopy, a novel optical spectroscopic approach was pursued to monitor the localized surface plasmon resonance (LSPR) of the gold nanoparticles. The nanoparticles were coated on the surface of poly isobutyl methacrylate (PiBMA) by physical vapor deposition. Subsequently, the LSPR spectra of nanoparticles on PiBMA were captured in a temperature-controlled optical cell in time series. A simple temperature control system was developed in the present thesis work, based on forced convective heating of the sample by Ar gas through the optical cell. Ar stream was heated in a glass capillary column inserted into an electrical resistance coil. The temperature is controlled by varying the electric current

and/or the Ar flow. The forced-convection heat transfer enables rapid stabilization of the temperature within seconds. The temperature was also measured at the sample surface using a K-type thermocouple.

The interaction of light with the conduction electrons in nanoparticles results in collective oscillations of the electrons which are known as localized surface plasmons (LSPs). LSPs can be resonantly excited by light at a certain frequency known as the plasmon frequency [18, 19]. Plasmon frequency will shift with the variation in dielectric constant of the surrounding medium. This spectral shift forms the basis of detection in LSPR sensors, which have found significant use in biomedical research in recent years [61, 62].

Maybe the most interesting attribute of the LSPR sensing is that it can monitor the dielectric variations around the nanoparticle within a few nm of the nanoparticle surface. Upon incidence of light, the metal nanoparticle acts as an optical antenna coupling with the incident photons in a spatial range comparable to its size [20]. In other words, photons coupled with the LSP localize to close vicinity of the nanoparticle creating enhanced electromagnetic near fields. As a result, LSPR is susceptible to the close vicinity of the nanoparticle, while the variation in LSPR can be reported to the far field in terms of scattering or absorption.

The impregnation or sinking of nanoparticles into the polymer is expected to cause spectral shift in LSPR of nanoparticles due to the changing dielectric environment surrounding nanoparticles. Because plasmon resonance fields are localized within a few nm from the nanoparticle surfaces, the signal will be selectively captured from the polymer region, which is within few nm of polymer/air interface.

On the other hand, if an objective lens is employed to probe the polymer surface by elastic/inelastic scattering or absorption, the spatial resolution is diffraction limited to the wavelength of light. Chapter 2 discusses this diffraction limitation of light in detail. In the visible spectrum, the shortest wavelength is about 400 nm. At this wavelength, the objective lens focused on the polymer surface will collect the optical signal from a minimum depth of 400 nm. Therefore, optical characterization of the polymer surface, which is the region within a few nm of the polymer/air interface, is practically out of question.

Hence, by the approach of the present thesis, diffraction limit of light can be overcome as the impregnation of nanoparticle into the polymer can be monitored to a spatial resolution down to a nanometer. As mentioned above, time series LSPR spectra of nanoparticle on PiBMA were acquired in transmission mode in a temperature controlled optical cell using a CCD spectrophotometer. The effective dielectric constant surrounding the

nanoparticle was calculated from LSPR optical extinction peak wavelength. Depth and velocity of penetration of nanoparticle were derived from the derived dielectric constant on the basis of normalized penetration depth.

A further advantage of the present approach lies in its being a non-contact technique. In the AFM technique employed by Teichroeb and Forrest, a contact probe is used to scan the polymer surface that can result in wetting of the AFM tip with the polymer as the polymer surface reaches T_g. Also, there is a chance of the AFM probe drifting the nanoparticles on the polymer surface. This drawback is overcome in the technique of the present thesis as no mechanical contact is needed.

The present thesis is organized as follows. Chapter 2 provides the background and literature review on deviation of T_{gs} of a polymer from bulk. It also furnishes the list of different methods followed by various groups in detecting the T_{gs} of polymers. Furthermore, it discusses the optical diffraction limit, a major setback in optical microscopy. This discussion is followed by the recent breakthroughs in overcoming this limit.

Chapter 3 develops the model for computing the normalized depth of penetration of nanoparticles into PiBMA surface from the variation in LSPR optical extinction spectra as a function of time.

Chapter 4 describes the experimental methodology including the temperature control of PiBMA surface by the temperature control system built at Oklahoma State University Functional Nanomaterials Laboratory.

Chapter 5 presents the time series LSPR spectra for embedding nanoparticles into PiBMA. The normalized depth of penetration vs. time was derived from the LSPR spectra using the model developed in chapter 3. Two types of measurements were conducted. First, the temperature was gradually increased from 25 to 70 °C at 5 °C increments maintaining the sample at each temperature for 10 min. The onset of nanoparticle penetration was found to be at 45 °C, which is 10 °C below the reported glass transition of PiBMA. Second, time series spectra were recorded at temperatures of 45, 55, 60, and 65 °C until saturation of the LSPR signal (i.e., end of penetration of nanoparticle). The activation energy for the penetration velocity was also derived.

Finally, conclusions are drawn and suggestions for future research are given in chapter 6.

CHAPTER 2

LITERATURE REVIEW AND BACKGROUND

Glass transition is observed in amorphous polymers. The T_g of polymers is defined as the temperature, at which a polymer experiences the transition from rigid to rubbery state with the increase of temperature [21]. Heating an amorphous polymer results in a polymer melt. Upon quench cooling, the molten polymer will be converted to glassy (amorphous) form. At a slower rate of cooling, the kinetic energy of molecules in the polymer cannot overcome the binding energy of the surrounding molecules and thus leads to the beginning of crystal formation. A fall in temperature further slows down the molecular motion resulting in a dynamic arrest of the molecules leading to the formation of a disordered glass at a certain temperature called the T_g. In the glassy state of a polymer, the atoms/molecules are prone to vibration only but not translational or rotational motion [77].

In 1994, Keddie, Jones and Cory first observed the deviation of polymer T_{gs} from bulk by experimenting on a 40 nm thick polystyrene film

deposited on a silicon substrate [5, 22]. This discovery stimulated significant interest in study and characterization of T_g in thin polystyrene films. The observations on T_{gs} of polymers led to the assumption that a visco-elastic layer with higher mobility exists on the surface of a polymer [22]. Studying the T_{gs} of a polymer by embedding metal nanoparticles have been a topic of great interest in recent years. Table I provides a list of techniques implemented by various groups to probe the T_{gs} of certain polymers by means of embedding metal nanoparticles. As seen in Table I, these studies had controversial findings [15-17, 22-27].

Table I. Various techniques implemented in probing the T_{gs} of polymers by embedding nanoparticles [15-17 & 23-26].

Year	Group	Technique	NPs	Polymer	Observations
2001	V. Zaporojtchenko, T. Strunskus, J. Erichsen and F. Faupel [23]	X-ray photoelectron spectroscopy	Copper (1-4 nm)	Polystyrene and Poly carbonate (0.5 – 2 μm)	$T_{gs} < T_{gb}$
2003	J. H. Teichroeb and J. A. Forrest [15]	Atomic Force Microscopy	Gold (10 and 20 nm)	Polystyrene (180 nm)	$T_{gs} < T_{gb}$
2003	R. Weber, I. Grotkopp, J. Stettner, M. Tolan and W. Press [24]	X-ray reflectivity	Gold (0.9 – 1.8 nm)	Polystyrene (80 – 100 nm)	$T_{gs} < T_{gb}$
2004	J. Erichsen, J. Kanzow, U. Schurmann, K. Doigner, K. Gunther-Schade, T. Strunskus, V. Zoporojtchenko, and F. Faupel [25]	XPS and small-angle X-ray scattering	Gold (2.2 – 2.6 nm)	Polystyrene (200 nm)	$T_{gs} < T_{gb}$
2005	S. A. Hutcheson and G. B. McKenna [16, 17]	Viscoelastic contact mechanics model	Gold (2.2-2.6 nm)	Polystyrene (200 nm)	$T_{gs} \approx T_{gb}$
2007	R. D. Deshmukh and R. J. Composto [26]	Transmission electron microscopy	Gold (20 nm)	Polystyrene (500–700 nm)	$T_{gs} > T_{gb}$

Accordingly, there are several open questions yet to be addressed:

1. Is T_{gs} equal or above or below T_{gb}?
2. If T_{gs} differs from T_{gb}, what is the distance from the polymer-air interface, where glass transition temperature is notably different than that in the bulk (T_{gb})?
3. What is the mechanical behavior of the polymer surface at a temperature equal or higher than T_{gs} but lower than melting temperature; is it viscous or visco-elastic? Is it possible to explain the so called "liquid layer" proposed by Teichroeb and Forrest [15] as the polymer, which is substantially above its T_g so that it behaves like a viscous liquid?
4. If the indentation of nanoparticles into polymer surface occurs below T_{gs}, why does it take minutes? Can the polymer wet the nanoparticle surface below T_{gs} and lead to surface energy reduction?

Therefore, a further investigation is essential to address the above questions.

In the present work, the LSPR of gold nanoparticles, which is characterized by optical extinction, plays a key role in probing T_{gs} of PiBMA. For a clear understanding of the method and principles involved, an intrinsic review of optical microscopy and recent breakthroughs in the field is appropriate at this juncture.

Optical microscopy has proven to be an invaluable tool for studying the microstructure. However, investigation of T_{gs} of a polymer requires a spatial resolution of 0.1 to 10 nm. Thus for studying this particular problem, one requires a microscopy technique whose resolution is of the order of at least 10 nm. Such a high resolution is impossible to attain in optical microscopy due to a fundamental limitation known as the "optical diffraction limit" [28-31].

It was Ernst Abbe in 1873, who deduced that the maximum resolution for an optical microscope is limited by the ability of its lens to focus a beam of incident light at a specific point ("focal point") [30]. Concentric circles appear at the focal point due to the phenomenon of diffraction. Hence, the distance between concentric circles defines the resolution limit of an optical microscope and is approximated by Abbe as

$$\boldsymbol{d = \frac{0.61\lambda_0}{n \sin \theta}} \qquad \textbf{(2.1)}$$

where, $\boldsymbol{d}$ is the distance between concentric circles, $\boldsymbol{\lambda_0}$ is the wavelength of light in vacuum, $\boldsymbol{n}$ is the refractive index of the medium, and $\boldsymbol{\theta}$ is the convergence angle of the incident beam of light for the lens. The denominator in Equation 2.1 $\boldsymbol{n \sin \theta}$ is defined as the numerical aperture of the optical system [30, 31]. The numerical aperture is mere a number that indicates the resolving power of a lens. The resolution of immersion microscopes has a slight

advantage over optical microscopes on the order of $\left(\frac{\lambda}{2n}\right)$. However, the increased resolution is limited to the available transparent materials with a small range of $\boldsymbol{n}$ [32-43].

For a period of time the only possible way to gain nanometer level spatial resolution for optical microscopy was to detect the evanescent optical waves in very close proximity of a studied sample using a scanning near-field optical microscope (NSOM) [44]. The high resolution NSOM has made it possible to image and map the LSPs [45]. NSOM is not affected by the optical diffraction limit. In general, NSOM has an optical fiber enclosed at one end with a metallic elongated sharp tip with a nanometer size opening. The Illumination is then introduced through this tip in order to scan the sample which is few nanometers away from the tip [46-51]. Thus, the optical resolution of NSOM is defined by the inner diameter of the tip. In order to achieve nano-scale optical images the tip is raster scanned over the sample by means of a piezoelectric drive through a scanning force microscope [52-54].

Even though high resolution can be achieved, NSOM is challenged by two major hurdles. First, designing a precise metal coated optical-fiber-tip with nano-scale interior diameter in order to allow the light sufficient enough for illuminating without causing damage to the sample is a difficult task. Second, the tunneling region of the probe is prone to intensity decays. These problems create challenges for analysis of data obtained through NSOM [55].

Furthermore, even though near-field optics still yields many interesting results, they are incomparable with the regular far-field optical microscopes in terms of specificity and convenience. Moreover, an image of a near-field optical microscope is obtained by indirect and extremely slow process of scanning the sample in a point-by-point manner [56]. The limitations of ordinary NSOM can be overcome by aperture-less NSOM. In the aperture-less NSOM technique, the scattered light is detected at the far field after the sample is illuminated at the near field by laser light through a sharp metallic probe. The optimized resolution of aperture-less NSOM owes to the optical field enhancement at and near the sample-probe tip region [57].

Discerning the optical properties of noble metal nanoparticles is of fundamental and practical importance [58]. According to quantum mechanics, a plasmon is created whenever a photon (light) is coupled to the coherent oscillation of conduction electrons. The LSP is a quasi-particle which lives only for ~10 fs and then disintegrates into a photon or phonons (i.e. heat). The disintegration or decay of a plasmon to photon is called “Scattering” while the decay of a plasmon to phonon(s) is called “Absorption”. The sum of absorption and scattering is called extinction.

Thus,

$$\boldsymbol{Extinction = Absorption + Scattering} \qquad \textbf{(2.2)}$$

When the frequency of an incident photon is in resonance with the frequency of collective oscillation of the conduction electrons, the noble metal nanoparticles exhibit a strong extinction band absent in the bulk metal spectrum [62]. This phenomenon is known as LSPR. The intensity and frequency of the extinction bands depend upon the size, shape and the medium surrounding the nanoparticles. The construction of various LSP based sensors rely on these important properties of the metal nanoparticles [63-70, 72-75].

The optical extinction of a metallic sphere in wavelengths much longer than the size of the sphere is deduced by Gustav Mie interpreting the optical properties of noble metal nanoparticles in relative simplicity and versatility which is discussed elaborately in chapter 3 of this thesis.

CHAPTER 3

THEORETICAL MODEL

In 1908, by fully solving for the Maxwell's Equations, Mie obtained an analytical solution for the extinction cross section of a solid sphere, $\boldsymbol{\sigma_{ext}}$, in an electromagnetic field of angular frequency $\boldsymbol{\omega}$. In case the sphere's diameter is significantly smaller than the wavelength of light (e.g., 20 times smaller), $\boldsymbol{\sigma_{ext}}$ is given by

$$\boldsymbol{\sigma_{ext}(\omega) = 9\frac{\omega}{c}\varepsilon_m^{3/2}V\left(\frac{\varepsilon_2(\omega)}{[[\varepsilon_1(\omega)+2\varepsilon_m]^2+[\varepsilon_2(\omega)]^2]}\right)} \quad \textbf{(3.1)}$$

where, $[\boldsymbol{\varepsilon_1(\omega) + i\varepsilon_2(\omega)}]$ and $\boldsymbol{\varepsilon_m}$ are the dielectric functions for the sphere and the surrounding medium, respectively [76]. $\boldsymbol{V}$ is the sphere's volume, and $\boldsymbol{c}$ is the velocity of light. $\boldsymbol{\sigma_{ext}}$ is defined such that, for a single nanoparticle, $\boldsymbol{P_{extinction} = I\sigma_{ext}}$, where $\boldsymbol{P_{extinction}}$ is the electromagnetic power coupled to the nanoparticle, which subsequently transforms it to re-emission (scattering) and/or heat (absorption) (i.e., extinction = absorption + scattering), and $\boldsymbol{I}$ is the incident irradiation (power per unit area).

Clearly, $\boldsymbol{\sigma_{ext}}$ has a resonance for

$$\boldsymbol{\varepsilon_1(\omega) + 2\varepsilon_m = 0, or\ \varepsilon_1(\omega) = -2\varepsilon_m,\ at\ \omega = \omega_{lsp},} \qquad \textbf{(3.2)}$$

that is known as the localized surface plasmon resonance (LSPR), while $\boldsymbol{\omega = \omega_{lsp}}$ is called the localized surface Plasmon (LSP) frequency. Obviously, $\boldsymbol{\omega_{lsp}}$ will shift with the variation in $\boldsymbol{\varepsilon_m}$. This forms the basis of detection for typical LSPR sensors. The real component of the dielectric function for the metals can be approximated as the sum of a term derived from free electron theory (plasmonic term) and a second term accounting for the deviations from the free electron behavior (i.e., interactions with atomic cores, intra-band and inter-band transitions), $\boldsymbol{\varepsilon_d}$, as:

$$\boldsymbol{\varepsilon_1(\omega) = 1 - \frac{\omega_p^2}{\omega^2} + \varepsilon_d} \qquad \textbf{(3.3)}$$

where $\boldsymbol{\omega_p}$ is the bulk plasmon frequency [76]. For gold, $\boldsymbol{\varepsilon_d}$ and $\boldsymbol{\omega_p}$ have been reported to be 10 and 6.97 eV, respectively [77]. Hence the resonance condition becomes

$$1 - \frac{\omega_p^2}{\omega_{lsp}^2} + \varepsilon_d + 2\varepsilon_m = 0 \qquad \textbf{(3.3a)}$$

$$\varepsilon_m = \frac{1}{2}\left(\frac{\lambda_{lsp}^2}{\lambda_p^2} - \varepsilon_d - 1\right) \qquad \textbf{(3.3b)}$$

where, $\lambda's$ denote the corresponding wavelengths. For an isolated gold nanosphere in vacuum $(\varepsilon_m = 1)$ the resonance wavelength, λ_{lsp}, is found to be $\lambda_{lsp} = \sqrt{13}\,\lambda_p$. Given $\lambda_p = 144$ nm for gold, λ_{lsp} is found as 520 nm [76].

The resonance frequency of gold nanoparticles coated on PiBMA is measured as 554 nm, which is red shifted from that of isolated nanoparticles. In other words, the effective ε_m is larger than 1, although the particles have not yet penetrated into the polymer. We attribute this higher value of ε_m to electromagnetic coupling between the nanoparticle and underlying polymer. Once the nanoparticle starts embedding into the polymer, the coupling with the polymer increases leading to a higher effective ε_m and increase in λ_{lsp}.

However, the interaction of the nanoparticle with the polymer during the embedding is dominantly in the near field as the polymer wets the surface of the nanoparticle. This near field coupling is due to strong concentration of photons (i.e., electromagnetic field) by the LSP mode, which is basically a

giant oscillating dipole. In a point dipole, the field decays as $(\mathbf{1}/\boldsymbol{d})^{\mathbf{3}}$, where $\boldsymbol{d}$ is the distance from the dipole center. Accordingly, the photon concentration decays as $(\mathbf{1}/\boldsymbol{d})^{\mathbf{6}}$. Hence, the electromagnetic coupling of the nanoparticle with its surroundings occurs in a skinny region, whose thickness is less than the radius of the nanoparticle.

If we only consider the polarization in the near field, the effective dielectric constant would be $\boldsymbol{\varepsilon_n}$. However, including the contribution due to polarization in the evanescent field, $\boldsymbol{\psi_e}$, the effective $\boldsymbol{\varepsilon_m}$ is:

$$\boldsymbol{\varepsilon_m = \varepsilon_n + \psi_e} \qquad \textbf{(3.4)}$$

Before embedding of the nanoparticle, there is no polymer wetting the nanoparticle surface. Hence $\boldsymbol{\varepsilon_n = 1}$ and $\boldsymbol{\varepsilon_m = \psi_e}$. An exact derivation of $\boldsymbol{\psi_e}$ is a challenging task that requires for a solution of the field distribution for a given penetration depth, $\boldsymbol{x}$. For convenience, we will consider $\boldsymbol{\psi_e}$ as constant and derive its value from the initial value of $\boldsymbol{\varepsilon_m}$ before embedding, $\boldsymbol{\varepsilon_{mo}}$ as:

$$\boldsymbol{\psi_e = \varepsilon_{mo} - 1} \qquad \textbf{(3.5)}$$

Second, we will derive $\boldsymbol{\varepsilon_n}$. To help with this derivation, a simple geometrical model for the embedding nanoparticle is illustrated in Figure 3.1. Here, a sphere of radius $\boldsymbol{R}$ is partially sunk in the polymer at a depth of $\boldsymbol{x}$.

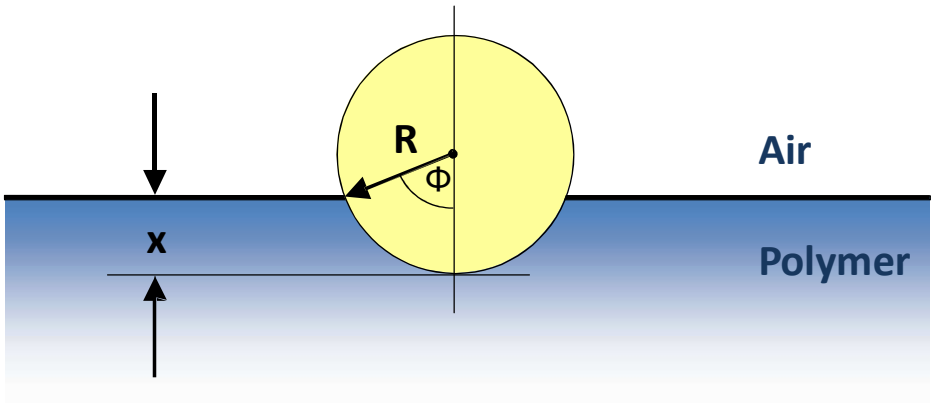

Figure 3.1. Schematics illustrating the sinking of a nanoparticle (NP) in a polymer.

To obtain an approximate expression for $\boldsymbol{\varepsilon_n}$, we will consider the vicinity of the nanoparticle, where field around the particle concentrated to. Electromagnetic coupling of the nanoparticle with its surroundings occurs in this skinny region surrounding the particle. Accordingly, a spherical shell of thickness $\boldsymbol{\delta}$ surrounding the nanoparticle is considered. $\boldsymbol{\delta}$ is significantly smaller than $\boldsymbol{R}$, the radius of the sphere. The average density of molecules, $\boldsymbol{N(x)}$, situated in this volume is given by

$$\boldsymbol{N(x) = \frac{N_p A(x) \delta}{4\pi R^2 \delta}} \qquad \textbf{(3.6)}$$

where $\boldsymbol{A(x)}$ is the surface area of the sphere in contact with the polymer, and $\boldsymbol{N_p}$ is the molecular density of the polymer. At full penetration, $\boldsymbol{N(x = 2R) = N_p}$. Further, $\boldsymbol{A(x)}$ may be calculated in terms of integration in spherical coordinates as:

$$A(x) = \int_{\theta=0}^{2\pi} \int_{\phi=0}^{\phi(x)} R^2 \sin\phi \, d\phi d\theta = 2\pi R x \quad (3.7)$$

In this integration, a fortunate relation is $R\cos\varphi(x) = R - x$, which simplifies its solution.

Therefore, Equation 3.6 resumes to

$$N(x) = \frac{1}{2} N_p(x/R) \quad (3.8)$$

The next step is to relate $\varepsilon_n(x)$ to $N(x)$ as:

$$\varepsilon_n(x) = 1 + \frac{N(x)\alpha}{\varepsilon_0} \quad (3.9)$$

where, N is the number of dipoles (e.g., mers) per unit volume, α is the molecular polarizability (i.e., for a mer), and ε_0 is the permittivity of the free space. Combining Equations 3.8 and 3.9 we get:

$$\varepsilon_n(x) = 1 + \frac{N_p\alpha}{\varepsilon_0}\left(\frac{x}{2R}\right) \quad (3.10)$$

Finally, combining Equations (3.4), (3.5) and (3.10)

$$\varepsilon_m(x) = \varepsilon_{mo} + \frac{N_p\alpha}{\varepsilon_0}\left(\frac{x}{2R}\right) \quad (3.11)$$

Upon complete embedding of the NP (i.e., $\boldsymbol{x = 2R}$), the effective dielectric constant reaches a value of $\boldsymbol{\varepsilon_{mf} = \varepsilon_m(2R) = \varepsilon_{mo} + \frac{N_p \alpha}{\varepsilon_o}}$. Therefore, $\boldsymbol{\frac{N_p \alpha}{\varepsilon_o} = \varepsilon_{mf} - \varepsilon_{mo}}$. Accordingly, Equation 3.11 can be rewritten as:

$$\boldsymbol{\varepsilon_m(x) = \varepsilon_{mo} + (\varepsilon_{mf} - \varepsilon_{mo}) \left(\frac{x}{2R}\right)} \quad \textbf{(3.12)}$$

Eventually, the penetration depth, $\boldsymbol{x}$, is found as

$$\boldsymbol{x = 2R \, \frac{\varepsilon_m(x) - \varepsilon_{mo}}{\varepsilon_{mf} - \varepsilon_{mo}}} \quad \textbf{(3.13)}$$

Therefore, the normalized penetration depth, $\boldsymbol{X = \frac{x}{2R}}$ can be written as:

$$\boldsymbol{X = \frac{\varepsilon_m(x) - \varepsilon_{mo}}{\varepsilon_{mf} - \varepsilon_{mo}}} \quad \textbf{(3.14)}$$

The same result was also derived by using dielectric mixing theory.

CHAPTER 4

EXPERIMENTAL PROCEDURE

4.1 Sample preparation

3 wt% PiBMA was dissolved in acetone by ultrasonication for 15 min and stored in a glass bottle with air tight seal. 1" × 1" Corning code 1737 glass substrates were first cleaned by brushing in 50% isopropyl alcohol in de-ionized water solution. The glass substrates were further cleaned in 100% isopropyl alcohol under ultrasonication for 15 min followed by thorough rinsing with de-ionized water and Ar blow dry. Finally, the substrate was placed on a hot plate at a temperature of 400 °C for 10 min to desorb the moisture.

Subsequently, the PiBMA solution was spin coated on the 1" × 1" glass substrates at 1500 rpm yielding approximately 200 nm thick films [71]. In order to evaporate the residual solvent and release the residual stress induced in the polymer film, it was cured for 20 hrs at 60°C on the hot plate, which is higher

than the T_{gs} of PiBMA (i.e., 55 °C).

The final sample preparation step involves coating of gold nanoparticles on the polymer by physical vapor deposition using Cressington 208 physical vapor deposition system equipped with a crystal thickness monitor. The deposition was carried out by melting a 0.49 g gold slug (obtained from Alfa Aesar) in a tungsten filament basket with a deposition rate of 0.1 nm/s. The current through the tungsten basket was recorded to be 33 A. The base pressure prior to gold deposition was $\sim 4\times10^{-5}$ Pa. The deposition was performed to a thickness of 0.8 nm.

4.2 Optical measurements

4.2.1 Extinction and Transmission

Transmission ($\boldsymbol{T}$) is given by $\boldsymbol{I/I_0}$, where $\boldsymbol{I}$ is the transmitted radiation and $\boldsymbol{I_0}$ is the incident radiation. The "Extinction" ($\boldsymbol{E}$) in optical spectroscopy is defined as the negative logarithm of $\boldsymbol{T}$ and is given by the following equation

$$\boldsymbol{E = -log(T)} \qquad \textbf{(4.1)}$$

When a beam of light is obstructed by a layer of nanoparticles, a fraction of electromagnetic power is absorbed and scattered by the nanoparticles whereas the rest is transmitted. In optical spectroscopy, since the absorbed or scattered photons (light) do not reach the detector of the spectrometer, these photons are called the "extinct" photons.

In a medium prone to photon extinction, the intensity of light decays exponentially in the direction of its propagation. In such a medium, the transmitted light is given by:

$$\boldsymbol{I = I_0 e^{-\alpha d}} \qquad \textbf{(4.2)}$$

Here, $\boldsymbol{I}$ & $\boldsymbol{I_0}$ are the intensities of the transmitted and incident light respectively, $\boldsymbol{\alpha}$ is the "extinction coefficient" and $\boldsymbol{d}$ is the distance traveled by the light. The extinction coefficient ($\boldsymbol{\alpha}$), is a measure of how strong a medium absorbs and scatters the light.

The extinction spectrum of the sample was determined using an optical spectrometer. Basically, an optical spectrometer consists of a light source, detector and a sample holder as shown in Figure 4.1. In the present study, a StellarNet EPP 2000Cs UV-Vis spectrometer (2048 pixel CCD detector, 2400 g/mm grating, 2 nm optical resolution, 200 μm slit size, deuterium + tungsten-

halogen light source) was employed for the optical extinction measurements of the sample. The sample was diced to 1" × 0.5" size and placed inside a glass optical cell. It was immobilized in the cell by a miniature steel spring. The optical cell is then placed inside the optical cell holder of the spectrometer for measuring the optical extinction. In order to maximize the signal to noise (S/N) ratio, the integration time was adjusted to 80 ms just avoiding the detector saturation. Recording of a single spectrum involved 50 accumulations.

In the present thesis work, optical extinction of gold nanoparticles (AuNPs) due to LSPR is key to studying the surface transition of the polymer. However, the recorded extinction spectrum is the sum of extinctions of the gold nanoparticles, optical cell, PiBMA and the glass substrate. Hence, the optical extinction of gold nanoparticles alone can be obtained by subtracting the extinction of PiBMA coated glass substrate without gold nanoparticles from the extinction of PiBMA coated glass substrate with gold nanoparticles. To consummate this operation, a reference (PiBMA coated glass substrate without gold nanoparticle deposition) was employed. Thus, the optical extinction of gold nanoparticles was obtained by subtracting the extinction of reference from the total extinction. In summary,

$$\boldsymbol{E_{total} = E_{Optical\,cell} + E_{AuNPs} + E_{PiBMA} + E_{Substrate}} \qquad \textbf{(4.3)}$$

$$E_{reference} = E_{Opticall\,cell} + E_{PiBMA} + E_{Substrate} \quad \textbf{(4.4)}$$

$$\therefore \quad E_{AuNPs} = E_{total} - E_{reference} \quad \textbf{(4.5)}$$

The above subtraction was performed by the SpectraWiz graphical user interface software of the optical spectrometer once E_{total} and $E_{reference}$ was obtained.

Two types of extinction measurements were conducted. First, the temperature was gradually increased from 25 to 70 °C at 5 °C increments maintaining the sample at each temperature for 10 min. When the polymer surface approaches T_{gb}, the gold nanoparticles begin to gradually sink into the polymer surface introducing an eminent shift in the optical extinction of nanoparticles due to variation in ε_m . Second, time series extinction spectra were recorded at temperatures of 45, 55, 60, and 65 °C until saturation of the LSPR signal (i.e., end of penetration of nanoparticle).

4.2.2 Temperature Control

As it follows from the above discussion, the present investigation requires a temperature control system that offers high precision and fast

stabilization. Since these requirements cannot be met by a hotplate or oven, a custom-made temperature control system was built.

The temperature control system comprises the following basic steps. First, Ar from the gas cylinder is allowed to flow through a heated glass tube as illustrated in Fig. 4.3. The tungsten coil wound around the tube provides the heating and is powered by a VARIAC. The VARIAC allows temperature control by varying the current through the heating coil. Subsequently heated Ar is guided to the optical cell containing the sample in order to maintain the polymer film at controlled temperature. The sample thus gets heated uniformly by means of forced convection heat transfer by Ar flow inside the optical cell. In addition, forced convection provides quick stabilization of the temperature. Finally, Ar flow exits the optical cell through an outlet needle. The flow rate of Ar was 125 cc/sec. A K-type thermocouple is inserted into the optical cell for monitoring the sample temperature. The tip of the thermocouple probe is positioned within 1 mm of the sample surface. The components of the temperature controller system are illustrated in Figs. 4.1, 4.2, and 4.3 and listed as follows:

- Heating glass tube: 7" length, 0.2" inner diameter (Fig. 4.3)
- Heating coil: 5" coiled length, 0.2" outer diameter (intact) (Fig. 4.3)
- HH11A digital thermometer with K-type thermocouple (KMQSS-010(G)-12, 12" length and 0.01" sheath diameter, grounded probe)

- 2 silicone rubber connecting tubes (3 ft and 6 ft)
- 2 16 G1 precision glide needles
- Vertical stand with two rubber clamps.

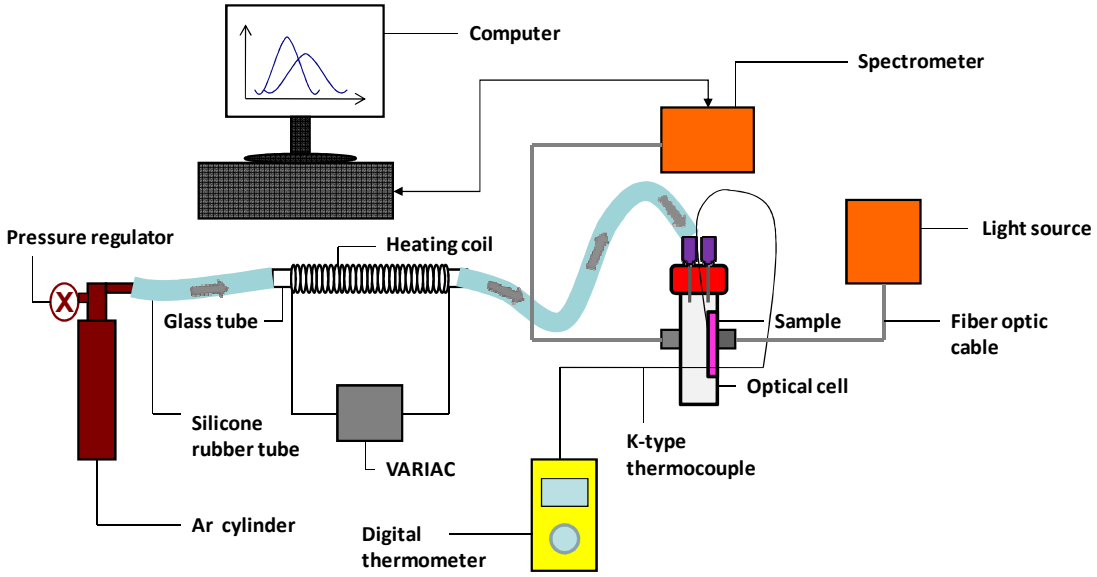

Figure 4.1. Illustration of the custom-made temperature control system.

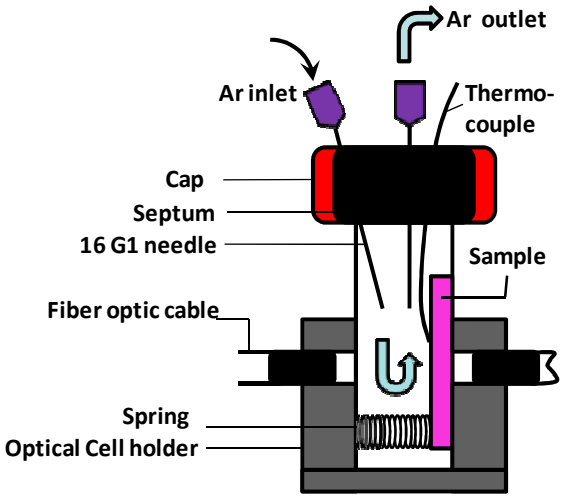

Figure 4.2. Schematic illustrating the temperature-controlled optical cell.

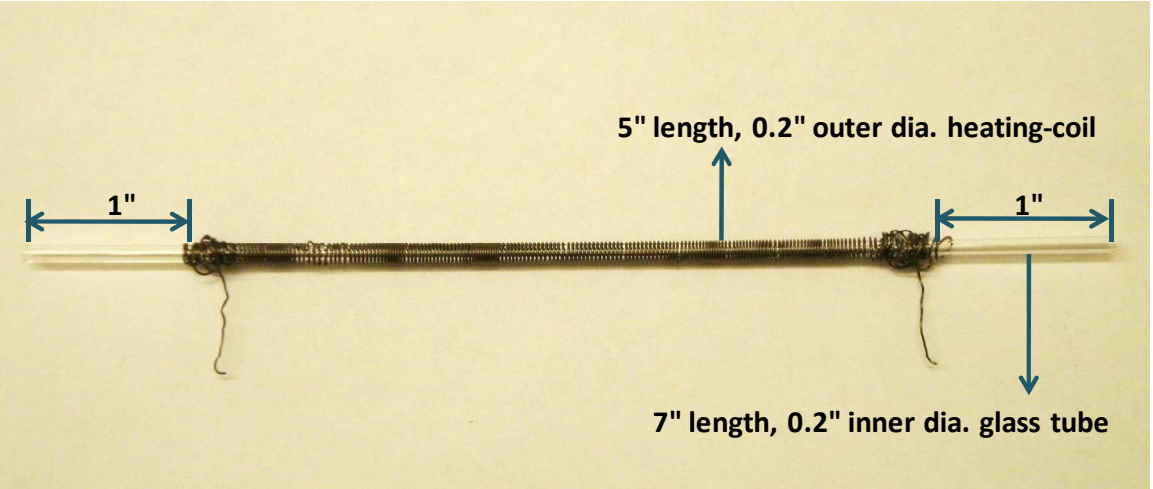

Figure 4.3. Photograph of the heating coil-wound-glass tube employed in the temperature-control system.

The glass tube was inserted into the heating coil making a firm contact leaving 1" bare- unwound edges of the tube on either side as shown in Figure 4.3. The glass tube along with the coil is held in a fixed horizontal position between two fiberglass coated clamps supported by the vertical stand. A 3 ft long silicone rubber tube connects the outlet of the compressed Ar supply to the inlet of the glass tube while a 6 ft long silicon rubber tube connects the outlet of glass tube to the inlet of the optical cell. The connection to the optical cell is through a 16 G1 needle pierced into the septum of the optical cell.

In addition, the K-type thermocouple probe was inserted into the optical cell through a temporary 16 G1 needle pierced into the septum. Once the

thermocouple probe tip was located near the sample surface, the temporary needle was removed. Finally the two terminals of the heating coil were connected to VARIAC power supply. This completes a home-made temperature control system required for the spectral acquisitions. During the measurement, the temperature showed minimal fluctuations and was maintained within ± 0.5 °C of the targeted temperature; i.e., of 45, 55, 60 and 65 °C.

4.2.3 Spectral Measurements

As mentioned earlier, optical extinction measurements were carried out in two ways: a) temperature series spectra by varying the temperature for a fixed sample; b) time series spectra at constant temperature for a fixed sample (conducted at 4 different temperatures).

A. Temperature series spectra:

After the sample was enclosed in optical cell and placed in cell holder the optical extinction spectra were recorded for incremental values of temperature beginning from a temperature lower than T_{gs} to a temperature higher than T_{gs} of the polymer. The time variation of the temperature was in "stairs-function" fashion, where the sample was kept at each temperature step for 10 minutes before a spectrum acquired. The optical extinction spectra remained stable until the temperature reached T_{gs} of the polymer beyond which the spectrum started to show a significant peak shift. When the optical extinction peak wavelengths were plotted against the temperature, a sudden

increase in the graph was observed on the temperature scale, thus revealing the glass transition of the polymer at the surface.

B. Time series spectra:

The spectrometer was set to capture time series spectra at a fixed temperature above T_{gs} of the polymer at a rate of 1 spectrum per min. The time series acquisition started once the temperature is stabilized to the targeted temperature. The stabilization typically took 25-30 sec. The acquisitions were performed for 4 different temperatures (i.e., 45, 55, 60 and 65 °C). As presented in Chapter 3, the present work has developed a normalized penetration depth model to analyze the time series extinction spectra and derive the sinking dynamics of the gold nanoparticles at the polymer surface at temperatures higher than T_{gs}.

CHAPTER 5

RESULTS AND DISCUSSION

5.1 Temperature series spectra

The initial investigation of the present work involved subjecting a gold nanoparticle coated polymer film (i.e., the sample) to a set of increasing temperatures from 25 to 70 °C with 5 °C increments. At each temperature step, the sample was maintained for 10 min before recording the optical extinction of gold nanoparticles. The extinction spectra are shown in Figure 5.1 and 5.2 and the corresponding peak wavelengths at the end of each temperature step is given in Figures 5.3.

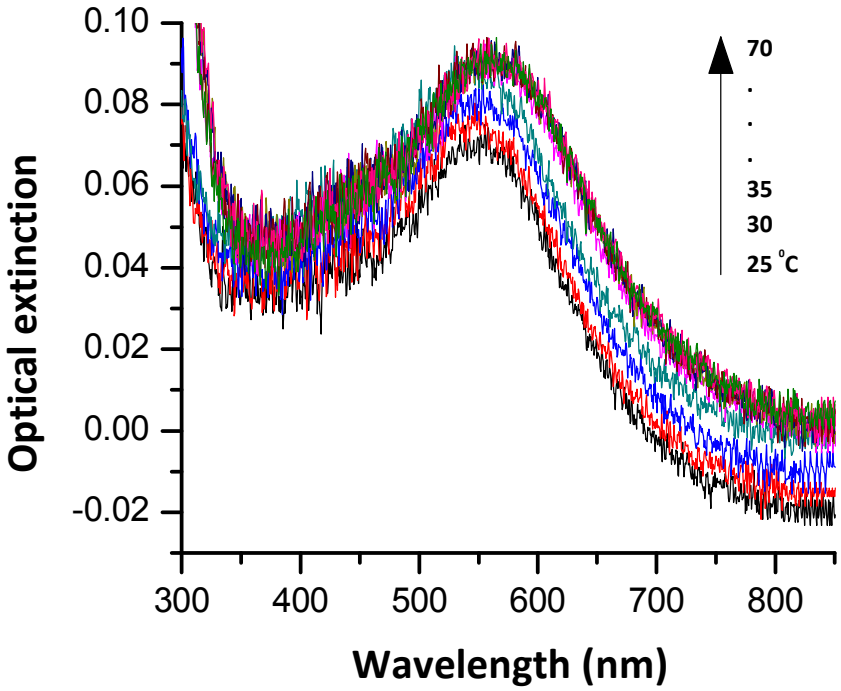

Figure 5.1. Temperature series optical extinction spectra of gold nanoparticles deposited on PiBMA.

Figure 5.1 exhibits a certain level of noise and hence the data is smoothened by Savitzky-Golay method and the resulting spectra is shown in Figure 5.2.

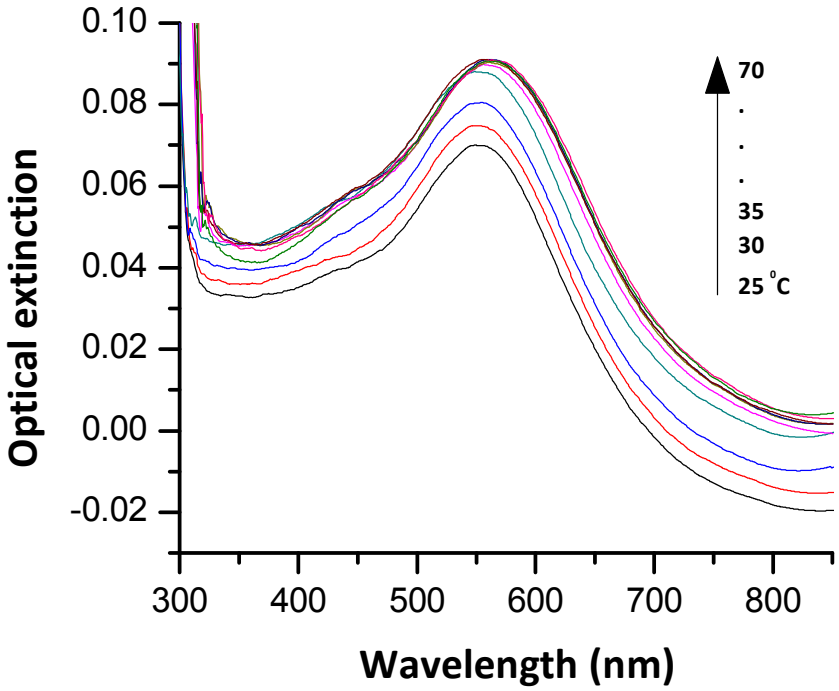

Figure 5.2. Smoothened data of temperature series spectra of gold nanoparticles deposited on PiBMA.

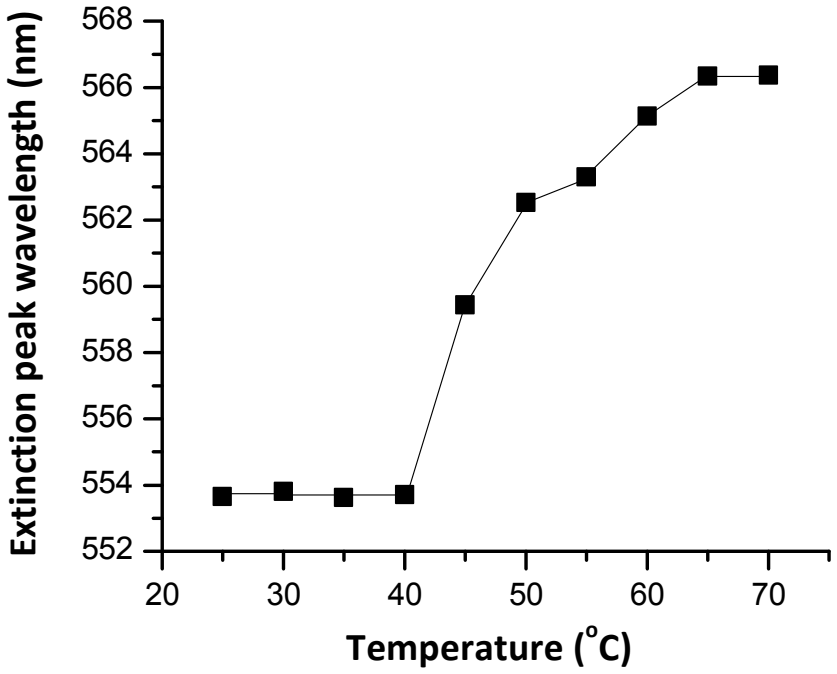

Figure 5.3. Optical extinction peak (wavelength) versus temperatiure of gold nanoparticles deposited on PiBMA.

From Figure 5.3, it is observed that the optical extinction peak wavelength of gold nanoparticles remains constant until the temperature of the sample reaches 40 °C. When the sample temperature is increased to 45 °C, the extinction peak wavelength undergoes a red shift of 4 nm. As stated in Chapter 3 of this thesis, a change in ε_m ω_{lsp} introduces a spectral shift in σ_{ext}. Thus, the observed peak shift at 45 °C suggests that there is a change in the surrounding medium of gold nanoparticles (i.e., a shift in ε_m) when the polymer temperature is incremented from 40 to 45 °C. The change in the surrounding medium of gold nanoparticles can be explained by embedding (at least partially) of the gold nanoparticle into polymer surface. In turn, this

embedding of the particles into polymer surface implies that the PiBMA surface experiences a transition from rigid to rubbery state between 40 and 45 °C. Hence by the definition of T_g of a polymer, the PiBMA surface reaches its T_g (T_{gs}) between 40 and 45 °C. The rubbery (i.e., viscous) state of the polymer surface allows the polymer flow around the nanoparticle and adsorb on the nanoparticle surface for minimization of the surface energy. Hence, the problem can be viewed as either embedding of nanoparticle into polymer surface or flow of polymer around nanoparticle. The driving force is the minimization of surface energy. In the rigid state of the polymer however, this process is kinetically inhibited and thermodynamic equilibrium cannot be established.

Interestingly, the data of Fig. 5.3 imply an offset of 10 °C or more between the T_{gs} (between 40 to 45 °C) and T_{gb} (55 °C). This finding is in agreement with Teichroeb and Forrest [15].

From Fig. 5.3 it is observed that when the temperature of the polymer is increased beyond 45 °C, the extinction peak shows further red shift until 65 °C. This observation suggests that at the end of the 45 °C exposure (10 minutes), the nanoparticles embed into the polymer only partially. Further, it is understood from the saturation of peak wavelength beyond 65 °C that the embedding stops sometime during the 65 °C anneal step. It is expected that saturation in the peak wavelength is indicative of complete embedding of gold

nanoparticles into PiBMA, because energy reduction should continue until all the nanoparticle surface is wetted by the polymer.

5.2 Time series spectra

In order to study the kinetics of gold nanoparticle penetration into PiBMA surface, time series LSPR optical extinction spectra of gold nanoparticles were acquired at four different temperatures at or higher than the T_{gs} of PiBMA i.e., at 45, 55, 60 and 65 °C.

Figure 5.6 shows the time series spectra of gold nanoparticles on PiBMA when they are exposed to 55 °C for 40 minutes. For a conspicuous glance of the peak shifts in time series spectra until the saturation, the data for the first 20 minutes of spectra was extracted from Fig. 5.4, smoothened and plotted in Fig. 5.5.

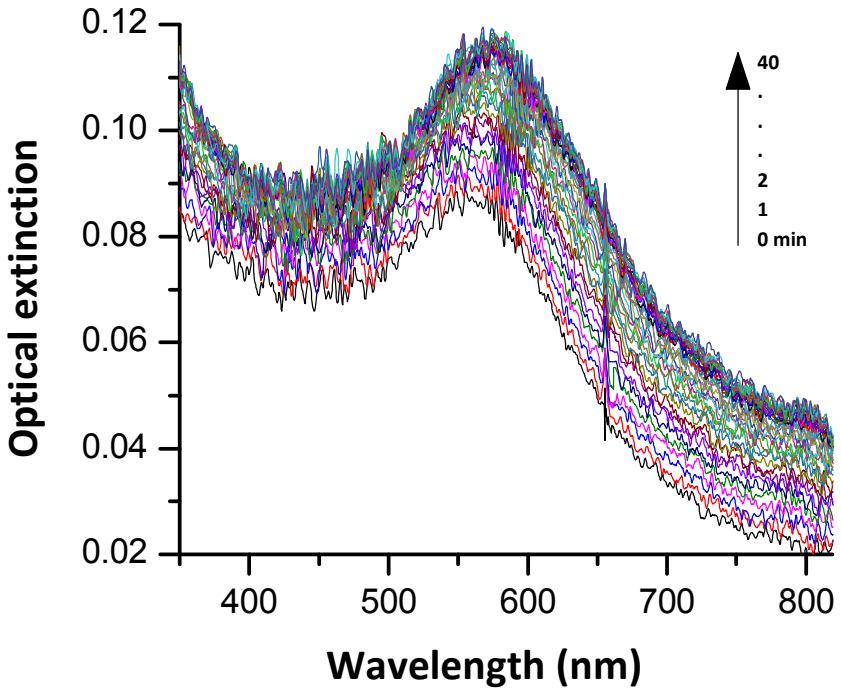

Figure 5.4. Time series LSPR optical extinction spectra of gold nanoparticles deposited on PiBMA at 55 °C.

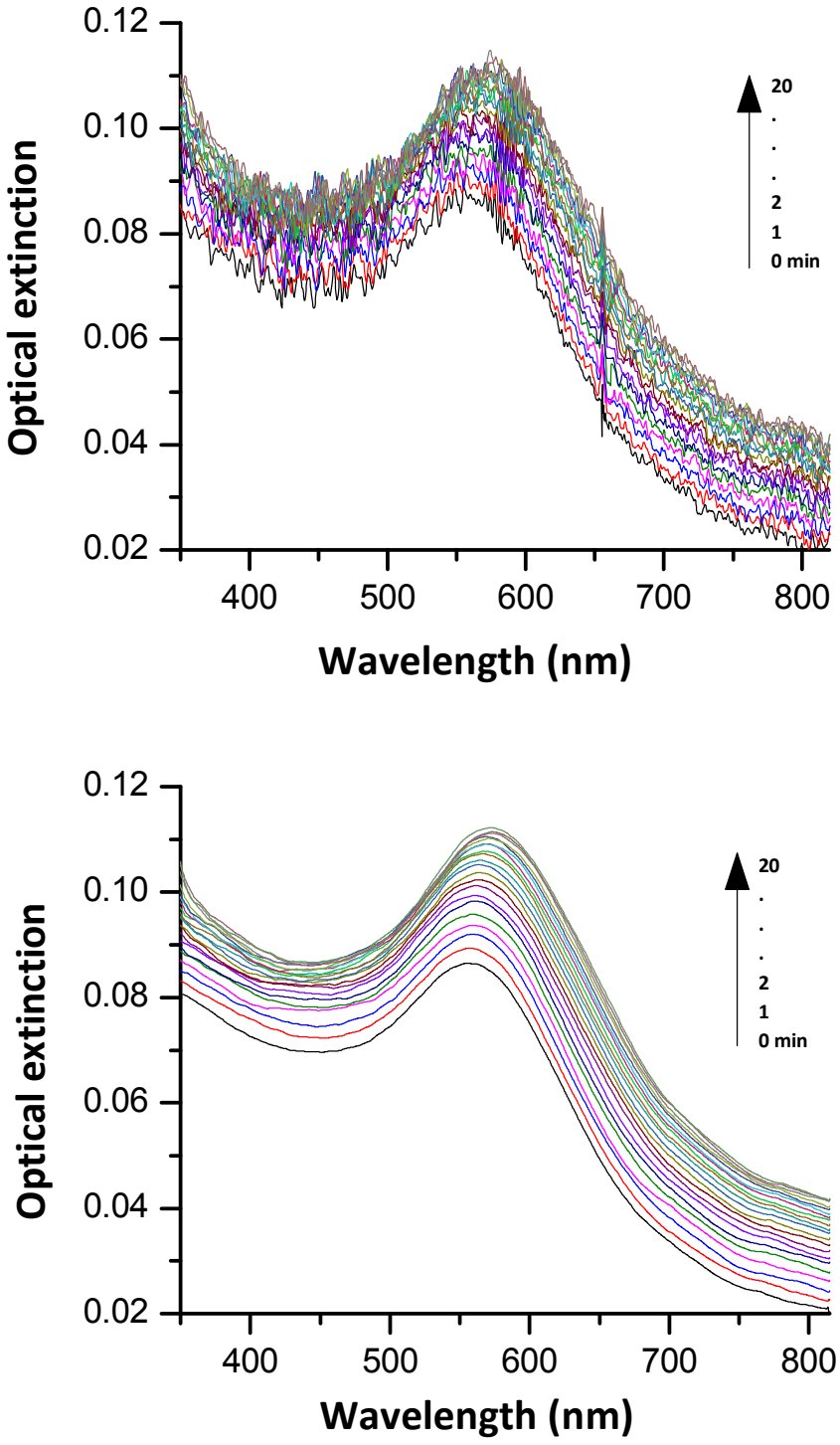

Figure 5.5. Original (top) and smoothened (below) time series extinction spectra of gold nanoparticles on PiBMA at 55 °C during the first 20 minutes.

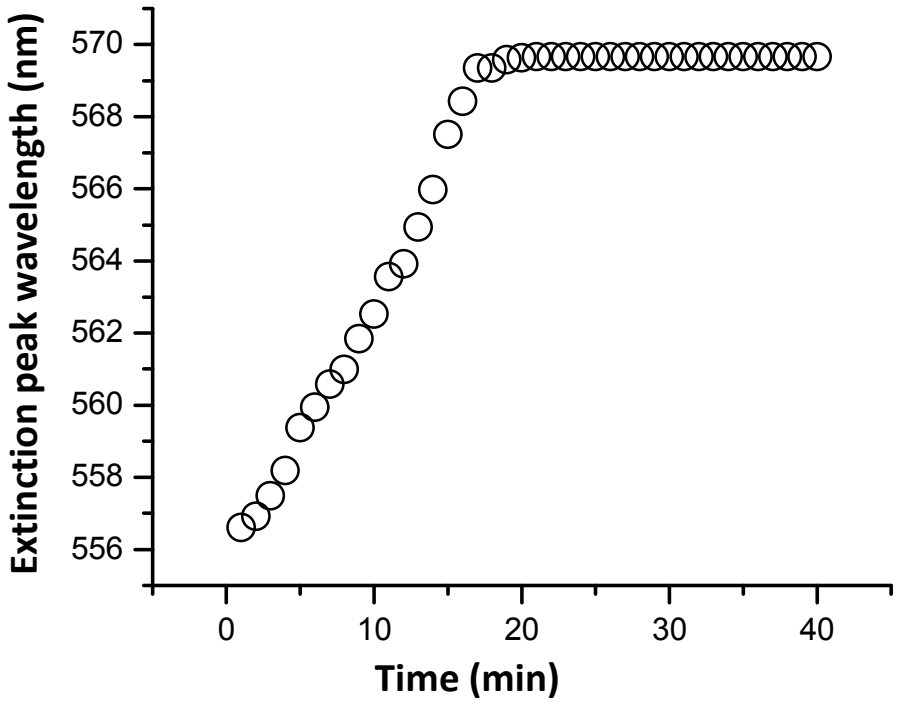

Figure 5.6. Peak shift in time series LSPR optical extinction spectra of gold nanoparticles deposited on PiBMA at 55 °C.

Figures 5.5 and 5.6 show time series optical extinction spectra of gold nanoparticles on PiBMA surface at 55 °C in 1 minute intervals for 40 minutes. It is seen that the peak wavelength shift is almost linear with time until the first 20 minutes which thereafter stops indicating the complete embedding of nanoparticles into the polymer.

Figure 5.7 shows the time series optical extinction of gold nanoparticles on PiBMA for 40 min at 60 °C. Figure 5.8 shows the smoothened data of Figure 5.7. And Figure 5.9 shows the corresponding shift of the extinction peak wavelength in 1-minute intervals. As in 55 °C, the peak shift is fairly linear with time. However, the peak shift lasts for a shorter duration of

14 minutes before saturation. Thus, the embedding speed increases with temperature that may be explained by reduced viscosity of the polymer.

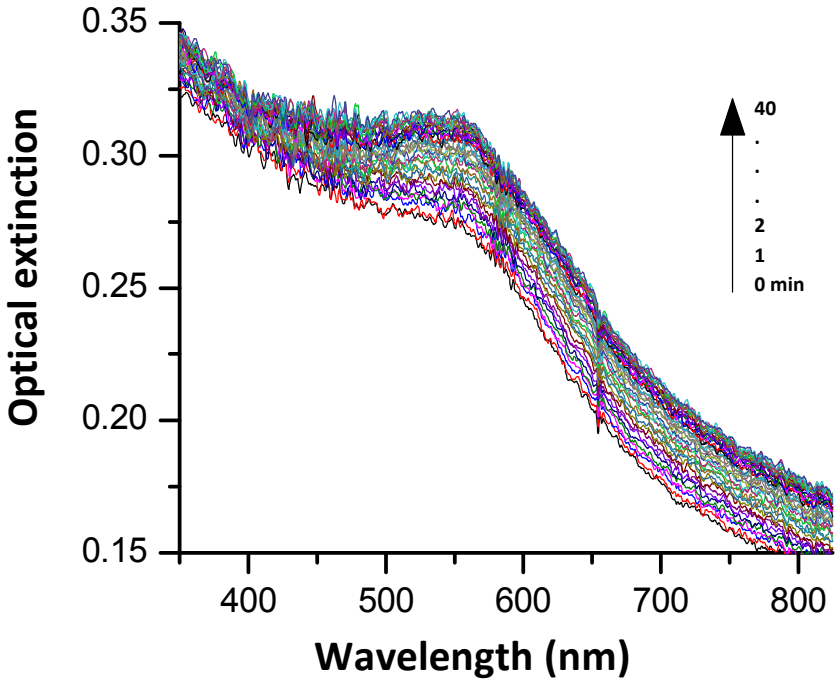

Figure 5.7. Time series LSPR optical extinction spectra of gold nanoparticles deposited on PiBMA at 60 °C.

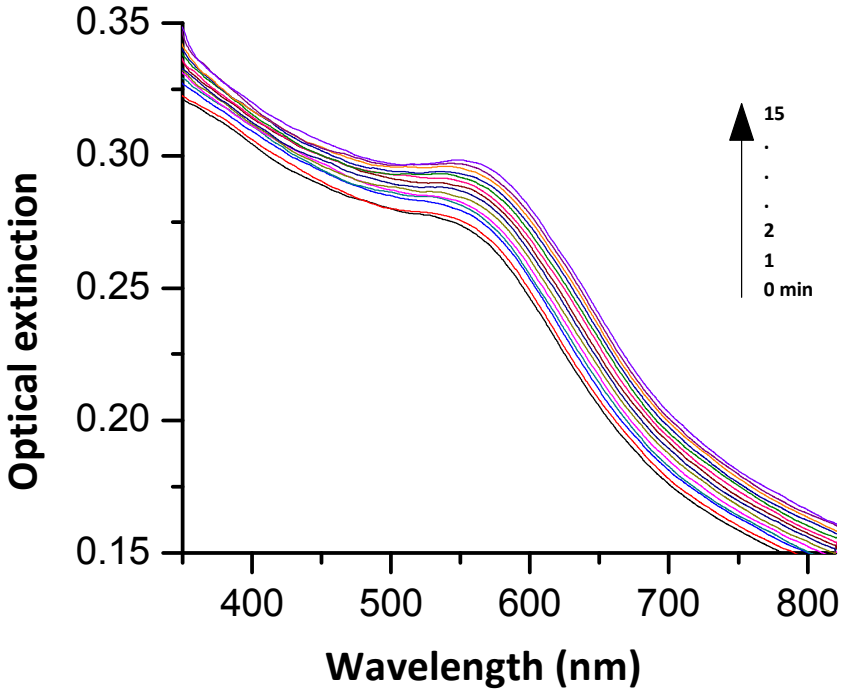

Figure 5.8. Smoothened time series extinction spectra of gold nanoparticles deposited on PiBMA at 60 °C.

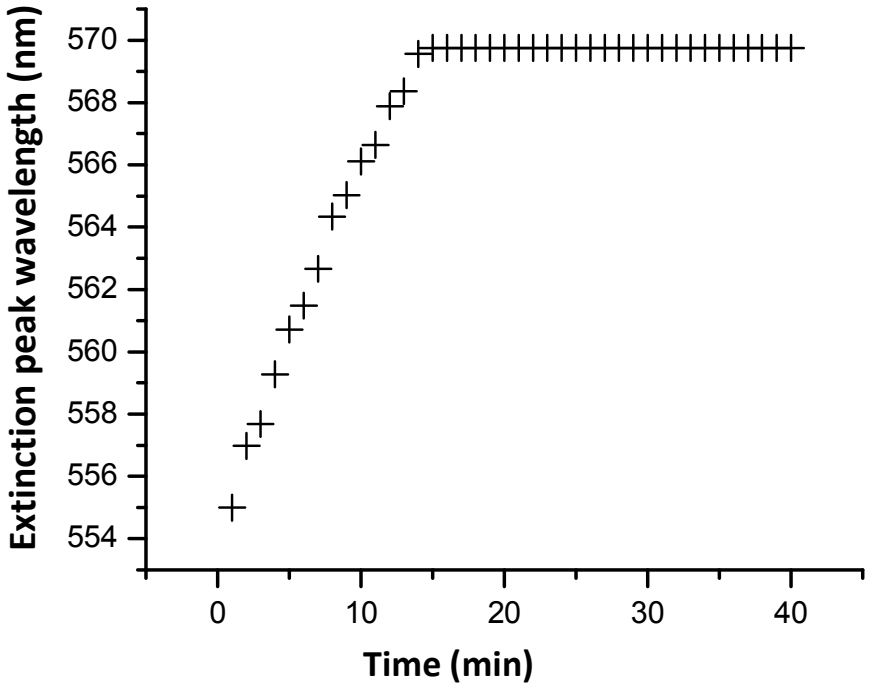

Figure 5.9. Peak shift in time series LSPR optical extinction spectra of gold nanoparticles on PiBMA at 60 °C.

Finally, Fig. 5.10 shows the time series extinction spectra of gold nanoparticles on PiBMA at 65 °C for 40 min. Figure 5.11 shows the smoothened plot of Figure 5.10 and Figure 5.12 shows the corresponding peak shift for each minute. It is evident in Figure 5.12 that the extinction peak wavelength shift with time is almost linear for 10 minutes, after which a point of saturation is reached indicating the completion of gold nanoparticle embedding into PiBMA surface.

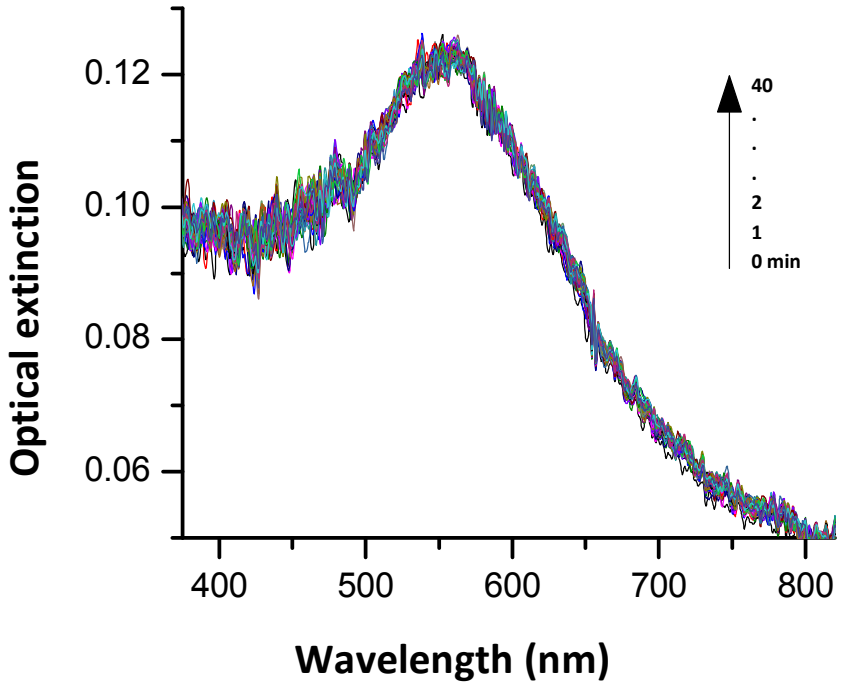

Figure 5.10. Time series LSPR optical extinction spectra of gold nanoparticles deposited on PiBMA at 65 °C.

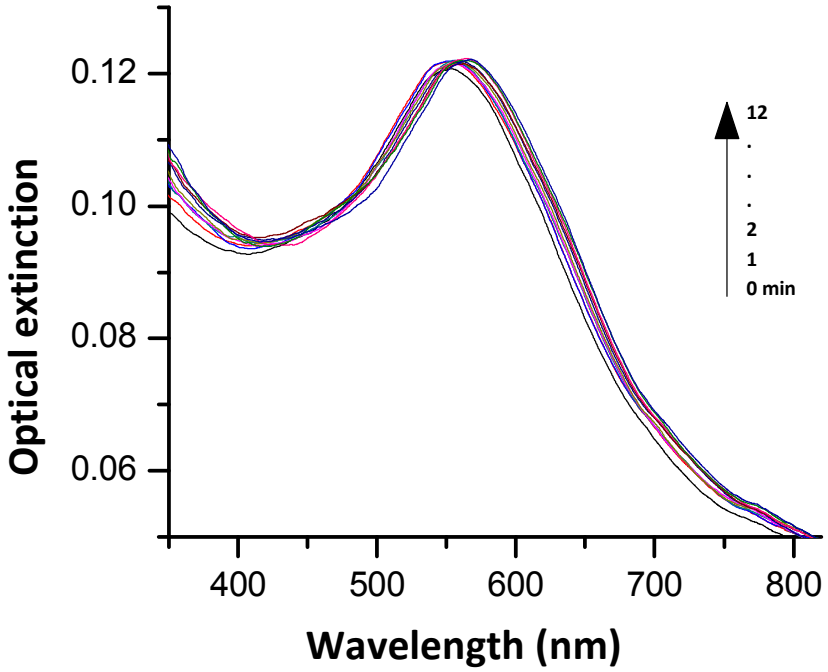

Figure 5.11. Smoothened time series extinction spectra of gold nanoparticles deposited on PiBMA at 65 °C.

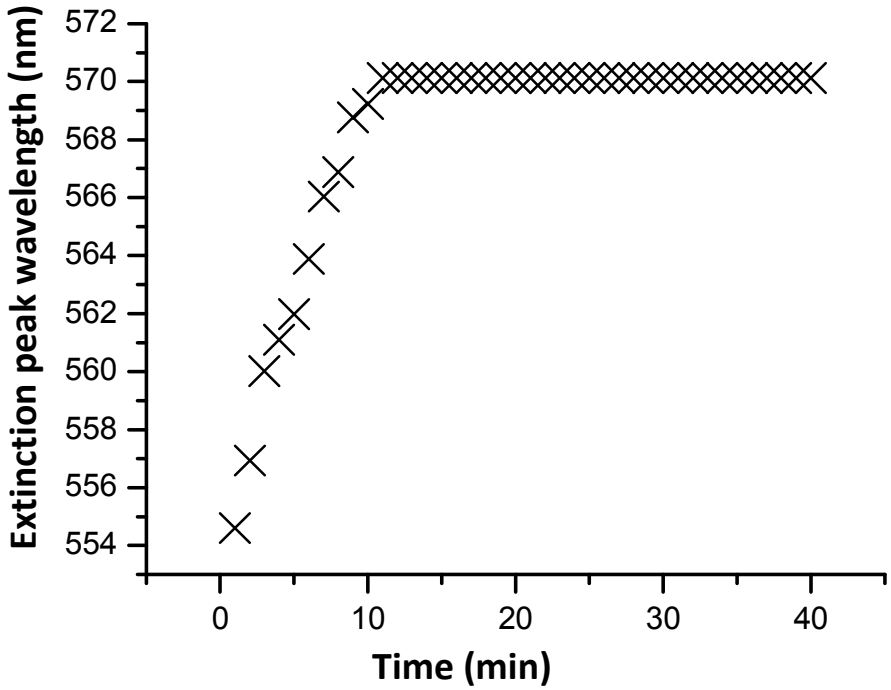

Figure 5.12. Peak shifts in time series LSPR optical extinction of gold nanoparticles deposited on PiBMA at 65 °C.

Figure 5.13 shows the time series extinction spectra of gold nanoparticles at 45 °C for a duration of 60 min.

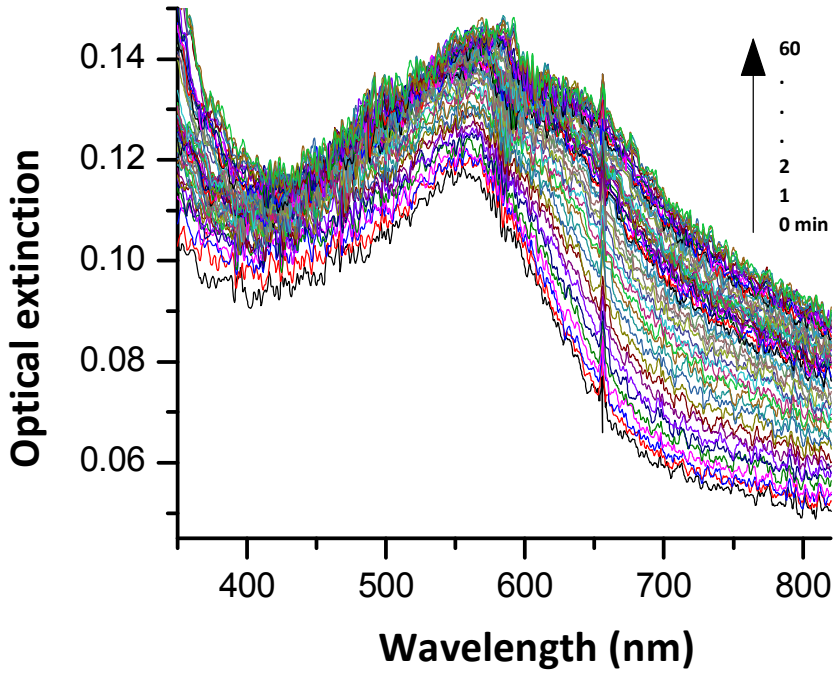

Figure 5.13. Time series LSPR optical extinction spectra of gold nanoparticles deposited on PiBMA at 45 °C.

Since the time series spectra in Figure 5.3 exhibit a certain noise level, the spectra were smoothened by Savitzky-Golay polynomial regression with the objective of accurate determination of the peak wavelength. The smoothened spectra are plotted in Fig. 5.14.

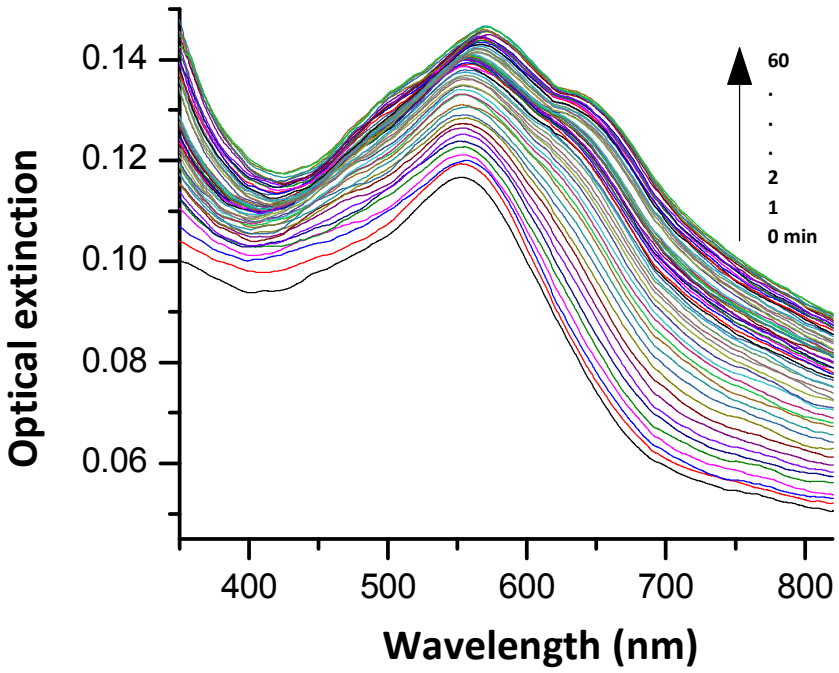

Figure 5.14. Time series extinction spectra of gold nanoparticles on PiBMA at 45°C after Savitzky-Golay smoothening.

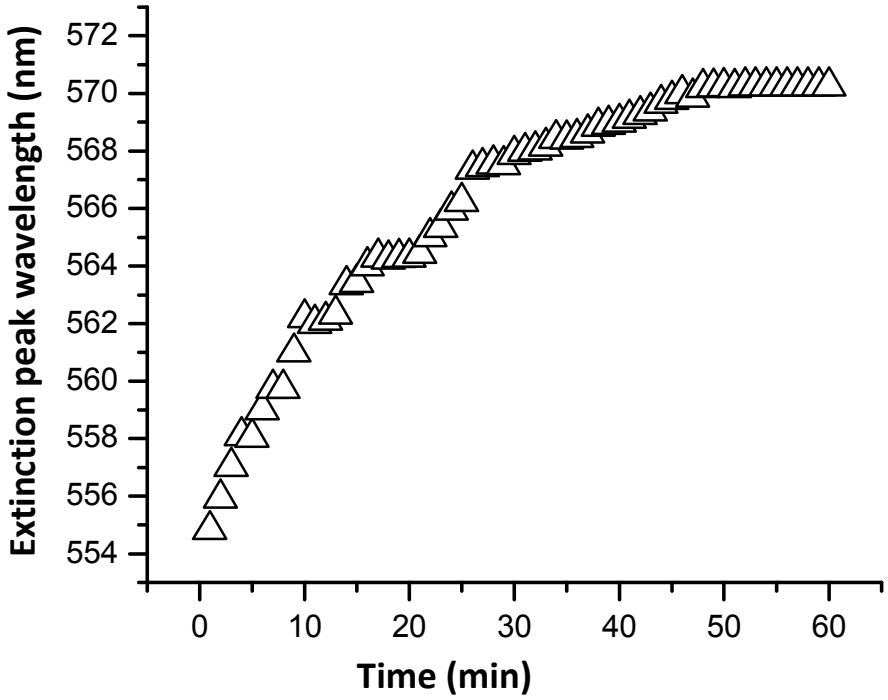

Figure 5.15. Extinction peak wavelength as a function of time at 45°C.

As depicted in Fig. 5.15, the extinction peak reaches a point of saturation (570 nm) at the 43rd minute that indicates the complete embedding of nanoparticles into polymer surface. In Figure 5.14, a second peak is observed to emerge at the 30th minute which thereafter continuously redshifts through the acquisition. This longer wavelength peak is not observed in the time series spectra of gold nanoparticles penetrating into PiBMA at higher temperatures. On the other hand, the shorter wavelength peak in Fig. 5.14 is found at around the same wavelength and saturates to the same wavelength as in higher temperature exposures. Therefore, the presence of two different plasmon resonance peaks in the extinction spectrum (Fig. 5.14) implies two different nanoparticle populations on the PiBMA surface. The shorter wavelength peak is associated with dispersed gold nanoparticle as in the temperature exposures of 55, 60, and 65 °C. On the other hand, the longer wavelength plasmon resonance peak must be associated with either a nanoparticle population penetrating into a region of significantly higher dielectric constant or a nanoparticle population experiencing aggregation. The former explanation suggests significant dielectric constant variations on the PiBMA surface at 45 °C. Because glass transition occurs in a range of temperatures and 45 °C is at the onset of this transition, one may expect property variations at the surface. However, previous work on the dielectric constant of polymers during glass transition demonstrated only minor variations [74]. Accordingly, we rule out the first explanation. The second explanation argues that NP aggregation is responsible for the longer wavelength peak. NP

aggregation leads to a red shifted plasmon peak due to particle-particle electromagnetic coupling (i.e., plasmon hybridization). This phenomenon is observed when the ratio of interparticle separation to particle diameter is reduced significantly below unity [75]. We argue that part of the nanoparticle population may experience aggregation when nanoparticle embedding rate is significantly nonuniform over the surface. At 45 °C, which is the onset of glass-to-rubber transition, it is likely that the polymer surface shows significant viscosity variations at the nanoscale. Therefore, some nanoparticles may experience slower or no penetration. Further, these slower particles may undergo lateral motion on the surface due to the flow patterns created by the sinking particles. In turn, this lateral movements may result in aggregation of the nanoparticles.

An interesting observation from Figure 5.15 is, even though the peak shift was observed to be linearly increasing with time there are eminent steps before saturation is reached. This step formation explains how the nanoparticles are not suddenly but gradually embedding into the PiBMA surface with time. One possible explanation to the gradual embedding of nanoparticles could be: the viscosity of the top most layer of the polymer surface may be decreasing with time thus resulting in the nanoparticle embedding into that particular surface layer. And, with further increase in time, the layer just beneath the top most surface layer could be becoming less viscous and thus resulting in further embedding of the gold nanoparticle. Thus the whole

process is continued until the saturation was reached at which the nanoparticle has completely embedded into the polymer surface.

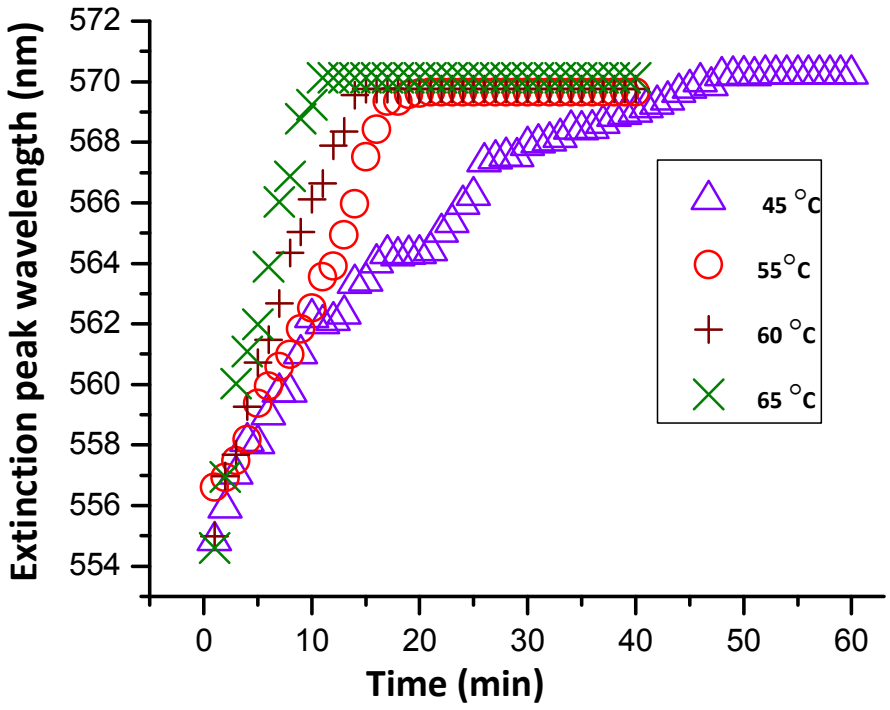

Figure 5.16. Peak shifts in time series LSPR optical extinction of gold nanoparticles deposited on PiBMA at 45, 55, 60 and 65 °C.

Figure 5.16 compares the kinetics of extinction peak wavelength (gold nanoparticles on PiBMA) for 4 different temperatures: 45, 55, 60 and 65 °C. A systematic increase of embedding rate of gold nanoparticles with temperature is inferred. As mentioned earlier, increased embedding rate is attributed to reduced viscosity of the polymer. Neglecting the inertial forces, the surface energy induced force on the nanoparticle must be balanced by the viscous force. Assuming a weak dependence of the surface energies on the temperature, the surface-induced force has no variation with temperature. So

does the viscous force. Because, the viscous force is a product of viscosity and shear rate (i.e., increases with embedding speed in this case), the increasing penetration rate with temperature suggests decreasing viscosity with temperature. Indeed, it is a well known fact that the viscosity of a polymer above its T_g decreases with increasing temperature. Figure 5.16 also shows the extinction peak saturates to the same wavelength of 570 nm irrespective of temperature. This result indicates the gold nanoparticle embed into the polymer at the same volume fraction independent of temperature. Most likely, nanoparticles embed into the polymer completely. Further, this result also suggests that the dielectric constant of the polymer has negligible variation in the range of 45 to 65 °C.

5.3 Calculating the normalized penetration depth (X) from the time series LSPR optical extinction spectra

Figure 5.17 shows the normalized penetration depth (X) for gold nanoparticle as they embed into PiBMA (i.e., as a function of time) for 4 different temperatures. Here, X values are calculated using Equation 14 of Chapter 3. X is the fractional contribution of the polymer to the effective dielectric constant around the nanoparticle that continuously increases as the nanoparticle embeds into the polymer. As it is derived in Chapter 3, X is fraction of the surface area wetted with the polymer, which turns out to be penetration depth divided by diameter for a spherical nanoparticle. However,

even before the embedding starts, at a temperature below T_{gs}, the nanoparticle has electromagnetic coupling with the polymer surface. It is evident from Fig. 5.17 that the $\boldsymbol{X}$ increases linearly with time for all 4 temperatures.

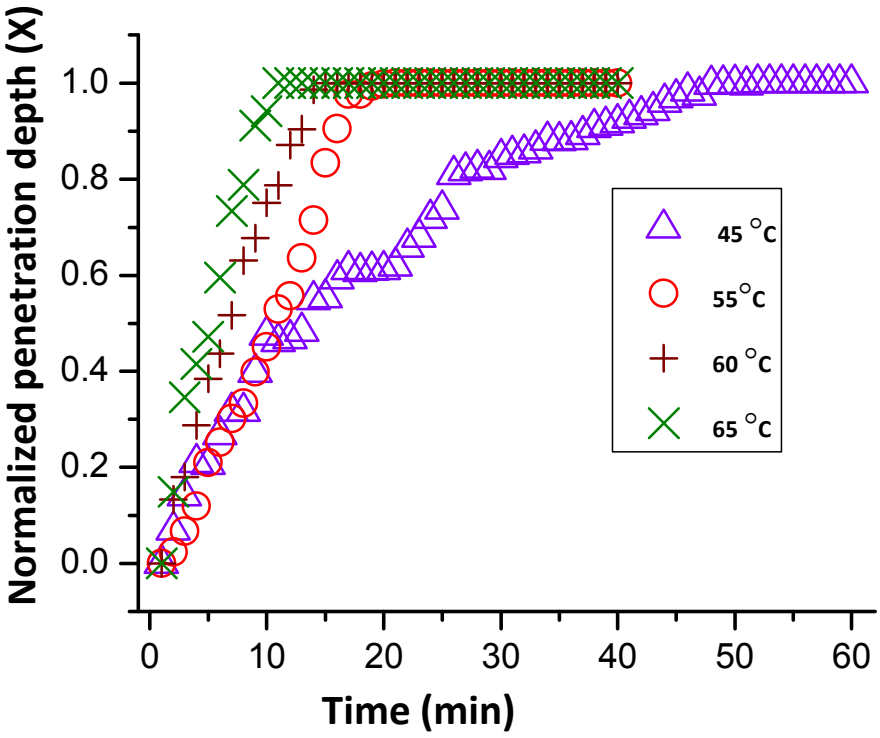

Figure 5.17. Average normalized penetration depth ($\boldsymbol{X}$) for the surrounding medium of AuNPs as they embed into PiBMA at 45, 55, 60 and 65 °C.

5.4 Calculating the average penetration depth from the time series LSPR optical extinction spectra

The average penetration depth for nanoparticles can be calculated using Equation 3.13 of Chapter 3 as: $\boldsymbol{x = 2RX}$ where, $\boldsymbol{X}$ is the normalized penetration depth and $\boldsymbol{x}$ is the depth of penetration of a nanoparticle into

polymer surface and $\boldsymbol{R}$ is the radius of the nanoparticle. Here, the averaging is over the nanoparticle population probed by the optical beam of 2 mm cross section. Furthermore, the average rate of depth of penetration of a nanoparticle can be calculated from the equation: $\boldsymbol{x^{\cdot} = 2RX^{\cdot}}$.

Figure 5.18 shows the semi- logarithmic relation between the penetration rate vs. $\frac{\boldsymbol{1}}{\boldsymbol{kT}}$ where, $\boldsymbol{k}$ is the Boltzmann's constant and $\boldsymbol{T}$ is temperature in Kelvin. The penetration rate values are derived from the data of Fig. 5.15 and based upon the linear regime. From the plot it is clear that the rate of penetration $\frac{\boldsymbol{1}}{\boldsymbol{kT}}$ reveals a Boltzman factor: $\boldsymbol{rate = Ce^{\left(\frac{-E_a}{kT}\right)}}$. This explains that the speed of nanoparticle penetration is thermally activated. The thermally activated nature of the embedding process may be explained by the requirement for displacement (i.e., flow) of the polymer at the vicinity of the nanoparticle while it is embedding. The displacement requires cleavage of the bonds between the polymer chains as well overcoming steric hindrances. Therefore, it is thermally activated. The activation energy, $\boldsymbol{E_a}$, is found to be 0.65 eV. From continuum point of view, as discussed earlier, thermally activated embedding speed can be explained by temperature dependence of the viscosity. Due to the inverse relation between speed and viscosity, an inverse Boltzmann factor for viscosity is inferred. Indeed, a number of publications in the literature report that the temperature dependence of viscosity in polymers is governed by an inverse Boltzmann factor:

The dynamic viscosity of the polymer can be related to the activation energy as [78],

$$\boldsymbol{\mu = Aexp(E_a/kT)} \qquad \textbf{(5.1)}$$

Where,

$\boldsymbol{E_a}$ = activation energy

$\boldsymbol{k}$ = Boltzmann constant, and

$\boldsymbol{T}$ = temperature in Kelvin.

$\boldsymbol{\mu}$= dynamic viscosity and

$\boldsymbol{A}$ = constant.

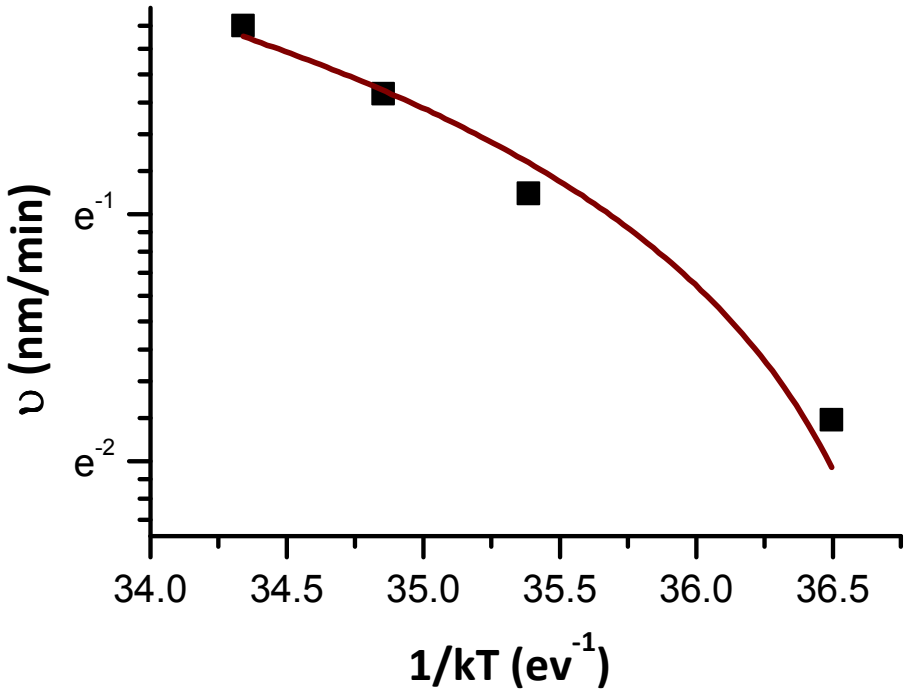

Figure 5.18. Rate of penetration of gold nanoparticles into PiBMA against $\boldsymbol{1/kT}$.

5.5 Driving force behind the embedding of a nanoparticle into the polymer surface

Following Hutcheson and McKenna, the force acting on a nanoparticle on a polymer surface, $\boldsymbol{F(t)}$, is given by [17] :

$$\boldsymbol{F(t) = 2\pi r(t)(\gamma_{SV} + \gamma_{LV} - \gamma_{SL})} \quad \textbf{(5.2)}$$

Where $\boldsymbol{r(t)}$ is the contact radius such that $\boldsymbol{2\pi r(t)}$ is the wetted perimeter of the nanoparticle by the polymer. $\boldsymbol{\gamma_{SV}}$, $\boldsymbol{\gamma_{LV}}$, $\boldsymbol{\gamma_{SL}}$ are the gold solid-vapor, polymer liquid-vapor and gold-polymer surface energies, respectively. Neglecting the gravitational and body forces, as well as the elastic force, $\boldsymbol{F(t)}$ must be in balance with a viscous force as:

$$\boldsymbol{F(t) = 2\pi r(t)(\gamma_{SV} + \gamma_{LV} - \gamma_{SL}) = \mu G(t)\dot{x},} \quad \textbf{(5.3)}$$

where $\boldsymbol{\mu}$ is the dynamic viscosity of the polymer and $\boldsymbol{A(t)G(t)}$ is a time varying function having the unit of length. $\boldsymbol{A(t)}$ $\boldsymbol{G(t)}$ is related to the geometry of the particle accounting for the viscous resistance. Accordingly, $\boldsymbol{A(t)G(t)}$ must relate to the geometry of the particle in contact with the polymer.

Since the experimental data in Figure 5.17 suggest that $\dot{x}$ is fairly constant with time, from Equation 5.3 it follows that the viscous force responsible for nanoparticle embedding is approximately of the form:

$$F_v(t) = C\mu r(t)\dot{x}, \tag{5.4}$$

where C is an appropriate unitless constant.

CHAPTER 6

CONCLUSIONS AND FUTURE WORK

The following conclusions were drawn from the results obtained in this thesis:

1. A novel technique is demonstrated where the T_{gs} of PiBMA was detected by the variation in LSPR optical extinction spectra of gold nanoparticles embedded on the polymer surface.
2. The shift in LSPR optical extinction peak wavelengths corresponding to the T_{gs} of PiBMA was observed at 10 °C less than the T_{gb} of PiBMA. Hence, we conclude that the T_{gs} of PiBMA is less than the T_{gb} of PiBMA.

3. Also as the results in Figures 5.1, 5.2 and 5.3, indicate that the polymer experiences the transition from rigid to rubbery state in the temperature zone of 45 °C to 65 °C, we conclude that the T_g of PiBMA is defined over a specific region and not at a specific point of temperature.
4. From the results obtained from the normalized penetration depth vs. time in Figure 5.14, which corresponds to the particle penetration into polymer surface we conclude that the nanoparticle penetration at all temperatures is linear with time. However, the rate of penetration is comparatively faster with increase in temperature i.e., the rate of nanoparticle penetration at 45 °C < 55 °C < 60 °C < 65 °C.
5. The saturation wavelength is same at 45, 55, 60 and 65 °C implying the same degree of nanoparticle embedding.
6. Since the experimental data in Figure 5.14 suggest that the rate of penetration, $\dot{x}$ is almost constant with time, it follows from equation 2 that the viscous force responsible for the nanoparticle embedding into polymer surface is approximately of the form: $\boldsymbol{F_v(t) = C\mu r(t)\dot{x}}$, where $\boldsymbol{C}$ is a constant, $\boldsymbol{\mu}$ is the dynamic viscosity, $\boldsymbol{r(t)}$ is the radius of the nanoparticle.
7. The speed of nanoparticle is thermally activated and the activation energy $(\boldsymbol{E_a})$ of PiBMA was derived and calculated as 0.5 eV.

In the present work, the nanoparticle was assumed to be a sphere and the effective dielectric constant of the surrounding medium of nanoparticle was calculated from averaging the dielectric constant over surface of the nanoparticle. However in actual practice since the size and shape of nanoparticles varies and due to which reason the effective dielectric constant also may vary considerably, the results obtained are close approximations. Studying an isolated single nanoparticle will eliminate these common problems encountered in the ensemble measurements such as the averaging on distribution of sizes, shapes, and structural defects (i.e. at interfaces) and even possible interaction effects between nanoparticles in the case of lower concentrations.

REFERENCES

[1] O. M. Leung and M. C. Goh, "Orientational ordering of polymers by atomic force microscope tip-surface interaction," *Science,* vol. 255, pp. 64-66, January 3, 1992.

[2] G. F. Meyers, B. M. DeKoven, and J. T. Seitz, "Is the molecular surface of polystyrene really glassy?," *Langmuir,* vol. 8, pp. 2330-2335, 1992.

[3] G. Reiter, "Mobility of Polymers in Films Thinner than Their Unperturbed Size," *EPL (Europhysics Letters),* vol. 23, p. 579, 1993.

[4] K. F. Mansfield and D. N. Theodorou, "Molecular dynamics simulation of a glassy polymer surface," *Macromolecules,* vol. 24, pp. 6283-6294, 1991.

[5] J. L. Keddie and et al., "Size-Dependent Depression of the Glass Transition Temperature in Polymer Films," *EPL (Europhysics Letters),* vol. 27, p. 59, 1994.

[6] G. Beaucage, *et al.*, "Ellipsometric study of the glass transition and thermal expansion coefficients of thin polymer films," *Journal of Polymer Science Part B: Polymer Physics,* vol. 31, pp. 319-326, 1993.

[7] W. J. Orts, *et al.*, "Observation of temperature dependent thicknesses in ultrathin polystyrene films on silicon," *Physical Review Letters,* vol. 71, p. 867, 1993.

[8] W.-l. Wu, *et al.*, "Film Thickness Dependent Thermal Expansion in Ultrathin Poly(methyl methacrylate) Films on Silicon," *Macromolecules,* vol. 28, pp. 771-774, 1995.

[9] A. M. Mayes, "Glass Transition of Amorphous Polymer Surfaces," *Macromolecules,* vol. 27, pp. 3114-3115, 1994.

[10] J. A. Hammerschmidt, *et al.*, "Probing Polymer Viscoelastic Relaxations with Temperature-Controlled Friction Force Microscopy," *Macromolecules,* vol. 32, pp. 3360-3367, 1999.

[11] T. Kerle, *et al.*, "Mobility of Polymers at the Air/Polymer Interface," *Macromolecules,* vol. 34, pp. 3484-3492, 2001.

[12] W. E. Wallace, *et al.*, "Influence of an impenetrable interface on a polymer glass-transition temperature," *Physical Review E,* vol. 52, p. R3329, 1995.

[13] X. P. Wang, *et al.*, "Surface Viscoelasticity Studies of Ultrathin Polymer Films Using Atomic Force Microscopic Adhesion Measurements," *Macromolecules,* vol. 34, pp. 4180-4185, 2001.

[14] S. Ge, *et al.*, "Shear Modulation Force Microscopy Study of Near Surface Glass Transition Temperatures," *Physical Review Letters,* vol. 85, p. 2340, 2000.

[15] J. H. Teichroeb and J. A. Forrest, "Direct Imaging of Nanoparticle Embedding to Probe Viscoelasticity of Polymer Surfaces," *Physical Review Letters,* vol. 91, p. 016104, 2003.

[16] S. A. Hutcheson and G. B. McKenna, "Nanosphere Embedding into Polymer Surfaces: A Viscoelastic Contact Mechanics Analysis," *Physical Review Letters,* vol. 94, p. 076103, 2005.

[17] S. A. Hutcheson and G. B. McKenna, "Erratum: Nanosphere Embedding into Polymer Surfaces: A Viscoelastic Contact Mechanics Analysis [Phys. Rev. Lett. 94, 076103 (2005)]," *Physical Review Letters,* vol. 94, p. 189902, 2005.

[18] Y. XIA, *et al.*, *Shape-controlled synthesis and surface plasmonic properties of metallic nanostructures*. Warrendale, PA, ETATS-UNIS: Materials Research Society, 2005.

[19] A. D. McFarland and R. P. Van Duyne, "Single Silver Nanoparticles as Real-Time Optical Sensors with Zeptomole Sensitivity," *Nano Letters,* vol. 3, pp. 1057-1062, 2003.

[20] P. Bharadwaj, *et al.*, "Optical Antennas," *Adv. Opt. Photon.,* vol. 1, pp. 438-483, 2009.

[21] W. D. Callister, Jr., *Material Science and Engineering: An Introduction,* 6th ed. New York: John Wiley, 2006.

[22] J. S. Sharp, *et al.*, "The properties of free polymer surfaces and their influence on the glass transition temperature of thin polystyrene films," *Eur. Phys. J. E,* vol. 15, pp. 473-487, 2004.

[23] V. Zaporojtchenko, *et al.*, "Embedding of Noble Metal Nanoclusters into Polymers as a Potential Probe of the Surface Glass Transition," *Macromolecules,* vol. 34, pp. 1125-1127, 2001.

[24] R. Weber, *et al.*, "Embedding of Gold Nanoclusters on Polystyrene Surfaces: Influence of the Surface Modification on the Glass Transition," *Macromolecules,* vol. 36, pp. 9100-9106, 2003.

[25] J. Erichsen, *et al.*, "Investigation of the Surface Glass Transition Temperature by Embedding of Noble Metal Nanoclusters into Monodisperse Polystyrenes," *Macromolecules,* vol. 37, pp. 1831-1838, 2004.

[26] R. D. Deshmukh and R. J. Composto, "Direct Observation of Nanoparticle Embedding into the Surface of a Polymer Melt," *Langmuir,* vol. 23, pp. 13169-13173, 2007.

[27] M. Ilton, *et al.,* "Using Nanoparticle Embedding to Probe Surface Rheology and the Length Scale of Surface Mobility in Glassy Polymers," *Macromolecules,* vol. 42, pp. 6851-6854, 2009.

[28] Abbe, E. *Arch. Mikrosk. Anat.,* vol. 9, pp. 413-468, 1873.

[29] R. C. Dunn, "Near-Field Scanning Optical Microscopy," *Chemical Reviews,* vol. 99, pp. 2891-2928, 1999.

[30] R. C. Dunn, "Near-Field Scanning Optical Microscopy," *Chemical Reviews,* vol. 99, pp. 2891-2928, 1999.

[31] E. BETZIG, *et al.*, "Breaking the Diffraction Barrier: Optical Microscopy on a Nanometric Scale," *Science,* vol. 251, pp. 1468-1470, March 22, 1991 1991.

[32] B. Hecht, *et al.*, "Scanning near-field optical microscopy with aperture probes: Fundamentals and applications," *Journal of Chemical Physics,* vol. 112, 2000.

[33] T. D. Harris, *et al.*, "Super-Resolution Imaging Spectroscopy," *Applied Spectroscopy,* vol. 48, pp. 14A-21A, 1994.

[34] R. Kopelman and W. Tan, "Near-Field Optical Microscopy, Spectroscopy, and Chemical Sensors," *Applied Spectroscopy Reviews,* vol. 29, pp. 39 - 66, 1994.

[35] D. Courjon and C. Bainier, "Near field microscopy and near field optics," *Reports on Progress in Physics,* vol. 57, p. 989, 1994.

[36] D. A. Vanden Bout, *et al.*, "Near-Field Optical Studies of Thin-Film Mesostructured Organic Materials," *Accounts of Chemical Research,* vol. 30, pp. 204-212, 1997.

[37] R. C. Dunn, "Near-Field Scanning Optical Microscopy," *Chemical Reviews,* vol. 99, pp. 2891-2928, 1999.

[38] E. BETZIG, *et al.*, "Breaking the Diffraction Barrier: Optical Microscopy on a Nanometric Scale," *Science,* vol. 251, pp. 1468-1470, March 22, 1991 1991.

[39] B. Hecht, *et al.*, "Scanning near-field optical microscopy with aperture probes: Fundamentals and applications," *Journal of Chemical Physics,* vol. 112, 2000.

[40] T. D. Harris, *et al.*, "Super-Resolution Imaging Spectroscopy," *Applied Spectroscopy,* vol. 48, pp. 14A-21A, 1994.

[41] R. Kopelman and W. Tan, "Near-Field Optical Microscopy, Spectroscopy, and Chemical Sensors," *Applied Spectroscopy Reviews,* vol. 29, pp. 39 - 66, 1994.

[42] D. Courjon and C. Bainier, "Near field microscopy and near field optics," *Reports on Progress in Physics,* vol. 57, p. 989, 1994.

[43] D. A. Vanden Bout, *et al.*, "Near-Field Optical Studies of Thin-Film Mesostructured Organic Materials," *Accounts of Chemical Research,* vol. 30, pp. 204-212, 1997.

[44] SUBRAMANIAM, *et al.*, *CELL BIOLOGICAL APPLICATIONS OF SCANNING NEAR-FIELD OPTICAL MICROSCOPY (SNOM)* vol. 44. Noisy-le-Grand, ROYAUME-UNI: Cellular and Molecular Biology, 1998.

[45] A. Lewis and K. Lieberman, "The optical near field and analytical chemistry," *Analytical Chemistry,* vol. 63, pp. 625A-638A, 1991.

[46] H. Heinzelmann, *et al.*, "Instrumental developments and recent experiments in near-field optical microscopy," *Thin Solid Films,* vol. 273, pp. 149-153, 1996.

[47] E. Betzig and R. J. Chichester, "Single Molecules Observed by Near-Field Scanning Optical Microscopy," *Science,* vol. 262, pp. 1422-1425, November 26, 1993 1993.

[48] R. C. Dunn, *et al.*, "Near-Field Fluorescence Imaging and Fluorescence Lifetime Measurement of Light Harvesting Complexes in Intact Photosynthetic Membranes," *The Journal of Physical Chemistry,* vol. 98, pp. 3094-3098, 1994.

[49] R. X. Bian, *et al.*, "Single Molecule Emission Characteristics in Near-Field Microscopy," *Physical Review Letters,* vol. 75, p. 4772, 1995.

[50] T. Ha, *et al.*, "Probing the interaction between two single molecules: fluorescence resonance energy transfer between a single donor and a single acceptor," *Proceedings of the National Academy of Sciences of the United States of America,* vol. 93, pp. 6264-6268, June 25, 1996 1996.

[51] R. Chang, *et al.*, "Theoretical investigation of near-field optical properties of tapered fiber tips and single molecule fluorescence," *Journal of Applied Physics,* vol. 81, pp. 3369-3376, 1997.

[52] C. E. Talley, *et al.*, "Single molecule detection and underwater fluorescence imaging with cantilevered near-field fiber optic probes," *Applied Physics Letters,* vol. 72, pp. 2954-2956, 1998.

[53] A. Bouhelier, *et al.*, "Plasmon-coupled tip-enhanced near-field optical microscopy," *Journal of Microscopy,* vol. 210, pp. 220-224, 2003.

[54] NOVOTNY, *et al.*, *Near-field optical microscopy and spectroscopy with pointed probes* vol. 57. Palo Alto, CA, ETATS-UNIS: Annual Reviews, 2006.

[55] N. F. Javad and et al., "Bow-tie optical antenna probes for single-emitter scanning near-field optical microscopy," *Nanotechnology,* vol. 18, p. 125506, 2007.

[56] B. A. Nechay, *et al.*, "Femtosecond near-field scanning optical microscopy," *Journal of Microscopy,* vol. 194, pp. 329-334, 1999.

[57] N. Dickenson, *et al.*, "Near-field scanning optical microscopy: a tool for nanometric exploration of biological membranes," *Analytical and Bioanalytical Chemistry,* vol. 396, pp. 31-43, 2010.

[58] T. Felicia and et al., "Controlling gold nanoparticle assemblies for efficient surface-enhanced Raman scattering and localized surface plasmon resonance sensors," *Nanotechnology,* vol. 18, p. 255702, 2007.

[59] C. E. H. Berger, *et al.*, "Surface Plasmon Resonance Multisensing," *Analytical Chemistry,* vol. 70, pp. 703-706, 1998.

[60] FRUTOS, *et al.*, *SPR of ultrathin organic films* vol. 70. Washington, DC, ETATS-UNIS: American Chemical Society, 1998.

[61] J. M. Brockman, *et al.*, "SURFACE PLASMON RESONANCE IMAGING MEASUREMENTS OF ULTRATHIN ORGANIC FILMS," *Annual Review of Physical Chemistry,* vol. 51, p. 41, 2000.

[62] K. F. Giebel, *et al.*, "Imaging of Cell/Substrate Contacts of Living Cells with Surface Plasmon Resonance Microscopy," *Biophysical Journal,* vol. 76, pp. 509-516, 1999.

[63] K. L. Kelly, *et al.*, "The Optical Properties of Metal Nanoparticles: The Influence of Size, Shape, and Dielectric Environment," *The Journal of Physical Chemistry B,* vol. 107, pp. 668-677, 2002.

[64] M. M. Miller and A. A. Lazarides, "Sensitivity of Metal Nanoparticle Surface Plasmon Resonance to the Dielectric Environment," *The Journal of Physical Chemistry B,* vol. 109, pp. 21556-21565, 2005.

[65] T. R. Jensen, *et al.*, "Nanosphere Lithography: Effect of the External Dielectric Medium on the Surface Plasmon Resonance Spectrum of a Periodic Array of Silver Nanoparticles," *The Journal of Physical Chemistry B,* vol. 103, pp. 9846-9853, 1999.

[66] J. Homola, *et al.*, "Surface plasmon resonance sensors: review," *Sensors and Actuators B: Chemical,* vol. 54, pp. 3-15, 1999.

[67] L. J. Sherry, *et al.*, "Localized Surface Plasmon Resonance Spectroscopy of Single Silver Nanocubes," *Nano Letters,* vol. 5, pp. 2034-2038, 2005.

[68] W. L. Barnes, *et al.*, "Surface plasmon subwavelength optics," *Nature,* vol. 424, pp. 824-830, 2003.

[69] R. C. Dunn, "Near-Field Scanning Optical Microscopy," *Chemical Reviews,* vol. 99, pp. 2891-2928, 1999.

[70] T. Klar*, et al.*, "Surface-Plasmon Resonances in Single Metallic Nanoparticles," *Physical Review Letters,* vol. 80, p. 4249, 1998.

[71] D. B. Hall*, et al.*, "Spin coating of thin and ultrathin polymer films," *Polymer Engineering & Science,* vol. 38, pp. 2039-2045, 1998.

[72] HAES*, et al.*, *Plasmonic materials for surface-enhanced sensing and spectroscopy*. Warrendale, PA, ETATS-UNIS: Materials Research Society, 2005.

[73] C. L. Nehl*, et al.*, "Scattering Spectra of Single Gold Nanoshells," *Nano Letters,* vol. 4, pp. 2355-2359, 2004.

[74] S. Link and M. A. El-Sayed, "Size and Temperature Dependence of the Plasmon Absorption of Colloidal Gold Nanoparticles," *The Journal of Physical Chemistry B,* vol. 103, pp. 4212-4217, 1999.

[75] M. A. v. Dijk*, et al.*, "Absorption and scattering microscopy of single Metal nanoparticles," *Physical Chemistry Chemical Physics,* vol. 8, pp. 3486-3495, 2006.

[76] U. Kreibig and M. Vollmer, *Optical Properties of Metal Cluster*: Springer, New York, 1995.

[77] N. R. Jadhav, V. L. Gaikwad, K. J. Nair and H. M. Kadam, "Glass transition temperature: Basics and application in pharmaceutical sector," *Asian Journal of Pharmaceutics,* vol. 3, pp. 82-89, 2009.

[78] E. V. Belyaeva and V. I. Sizov, "Connection between the activation energy of viscous flow and the composition of electric steel melting slags during the production of various types of steel," *Refractories and Industrial Ceramics,* vol. 23, no. 11, pp. 47-50, Nov 1982.

VITA

Ratan Kishore Putla

Candidate for the Degree of

Master of Science

Thesis: **MONITORING OF GLASS TRANSITION AT A POLYMER SURFACE BY LOCALIZED SURFACE PLASMON RESONANCE.**

Major Field: Mechanical and Aerospace Engineering

Biographical:

Personal Data: Born **18th June 1984**, **Hyderabad, India**

Education:

Completed the requirements for the Master of Science in Mechanical and Aerospace Engineering, Oklahoma State University, Stillwater, Oklahoma in December, 2010.

Completed the requirements for the Bachelor of Technology in Mechanical Engineering at Jawaharlal Nehru Technological University, Hyderabad, India in 2006.

Experience:

1. Graduate Research Assistant, Mechanical and Aerospace Engineering, OSU (May 2007 – May 2010).
2. Graduate Teaching Assistant, Mechanical and Aerospace Engineering, OSU (January 2007 – May 2008).
3. Graduate Teaching Assistant, Department of Physics, OSU (January 2009 – May 2009 and August 2010 – December 2010).
4. Graduate Tutor, College of Engineering, Architecture and Technology, OSU (January 2010 – May 2010)

Professional Memberships:

1. Member of American Society of Mechanical Engineers.
2. Member of National Scholars Honors Society.

Name: **Ratan Kishore Putla** Date of Degree: **December 2010**
Institution: **Oklahoma State University** Location: **Stillwater, Oklahoma**

Title of Study: **MONITORING OF GLASS TRANSITION AT A POLYMER SURFACE BY LOCALIZED SURFACE PLASMON RESONANCE**

Pages in Study: **65** Candidate for the Degree of **Master of Science**

Major Field: **Mechanical and Aerospace Engineering**

Scope and Method of Study:
The present work investigates glass transition on a polymer surface by embedding gold nanoparticles into the polymer and exploiting the localized surface plasmon resonance (LSPR) of the nanoparticle as the probe. The impregnation of nanoparticles into polymer causes a spectral shift in LSPR due to the changing dielectric environment surrounding nanoparticles. LSPR is sensitive to the close vicinity of nanoparticles within a few nm from the nanoparticle surface. Therefore, the diffraction limit of light can be beaten by orders of magnitude and impregnation of nanoparticles into the polymer can be monitored to a spatial resolution down to a few nm.

Findings and Conclusions:
Gold nanoparticles at an average size of 8 nm, were synthesized on poly isobutyl methacrylate (PiBMA) films on glass by physical vapor deposition. Subsequently, time series LSPR spectra of nanoparticle on PiBMA were acquired in transmission mode in a temperature controlled optical cell using a CCD spectrophotometer. The forced convective heating of the sample by Ar gas through the optical cell enables rapid stabilization of the temperature in few seconds. The temperature was measured at the sample surface by a K-type thermocouple. The effective dielectric constant surrounding the nanoparticle was calculated from LSPR optical extinction peak. Depth and velocity of penetration of nanoparticle were derived from the measured dielectric constant on the basis of dielectric mixing. Two types of measurements were conducted. First, the temperature was gradually increased from 25 to 70 ºC at 5 ºC increments maintaining the sample at each temperature for 10 min. The onset of nanoparticle penetration was found to be at between 40 and 45 ºC, which is below the reported glass transition of PiBMA by 10 to 15 ºC. Second, time series spectra were recorded at temperatures of 45, 55, 60, and 65 ºC until saturation of the LSPR signal (i.e., end of penetration of nanoparticle). The penetration velocity was found to be fairly constant in time while temperature activated at an energy of 0.65 eV.

Name: **Ratan Kishore Putla** Date of Degree: **December, 2010**
Institution: **Oklahoma State University** Location: **Stillwater, Oklahoma**

ADVISER'S APPROVAL: **Dr. A. Kaan Kalkan**

ADVISER'S APPROVAL: **Dr. A. Kaan Kalkan**